Biophysical Chemistry, 43 (1992) 279–310
Elsevier Science Publishers B.V., Amsterdam

DNA associations: Packing calculations in A-, B-, and Z-DNA structures

A.R. Srinivasan and Wilma K. Olson

Department of Chemistry, Rutgers, the State University of New Jersey, New Brunswick, NJ 08903 (USA)

(Received 12 November 1991; accepted in revised form 17 February 1992)

Abstract

A detailed theoretical study has been carried out to examine the modes of DNA–DNA interactions on the basis of hard-sphere contact criteria. Two helices of identical structure and length are oriented side-by-side and their relative positions are controlled by translations along and rotations about specific axes. Short atomic contacts between pairs of atoms in the structures are assessed and contact-free configurations are compiled. The computed contact-free arrangements of A, B, and Z double helices are found to be remarkably similar to the packing motifs observed in DNA crystals and stretched fibers. Equally interesting in the study are the broad ranges of sterically acceptable arrangements that preserve the overall packing morphology of neighboring duplexes: Among the most notable morphological features in the helical complexes are extended "super" major and minor grooves which might facilitate the wrapping and packaging of DNA chains in supramolecular assemblies. The hard-sphere computations, however, are insufficient for quantitative interpretation of the packing of DNA helices in the solid state. The results are, nevertheless, a useful starting point for energy based studies as well as relevant to the analysis of long-range interactions in DNA supercoils and cruciforms.

Keywords: DNA associations; Crystal packing; A-, B-, Z-DNA; Hard-sphere contacts

1. Introduction

The recent surge of activity in the areas of DNA condensation and interactions has provided several clues to the nature of the packaging of the double helix within the narrow confines of the cell. In order to conform to the observed dimensions of the nucleus, the DNA must fold into compact spatial arrangements only a fraction of the extended helical contour length. The chain molecule must also associate in an organized manner, which in some organisms (e.g., bacteria, dinoflagellates, mitochondria) appears to resemble a cholesteric liquid crystal [1–3]. While several models of chain folding have been developed to account for the apparent compaction of isolated helices in protein-nucleic acid complexes [4–8] or in solution [9–13], much less is known at the molecular level on the dense packing of DNA strands.

Current information on the packing of DNA at the molecular level is derived from a variety of model studies of polymer aggregates in both aqueous solution and the solid state. The strong circular dichroism signals of cation and polymer condensed DNA suspensions, for example, are indicative of a higher-order liquid crystalline-like

Correspondence to: Prof. W.K. Olson, Department of Chemistry, Rutgers, the State University of New Jersey, New Brunswick, NJ 08903 (USA).

organization in these aggregates [14–16]. At moderate polymer concentrations the liquid crystalline phase is cholesteric [1,17–19], while at high concentrations it is columnar hexagonal [20]. In such systems, the end-over-end tumbling of the DNA duplex is restricted by close packing, although short chains are apparently able to twist about their long axes [21]. The chains in liquid crystalline phases also exhibit a characteristic cholesteric helical pitch [22], presumably related to interstrand packing. According to osmotic pressure measurements of polymer-condensed DNA in 0.005–1.0 *M* ionic solutions [23,24], adjacent double helices are separated by interaxial distances of 25–45 Å. The collapsed DNA's visualized in freeze fracture electron microscopic preparations of large torus shaped aggregates are packed at comparable distances [25], as are the DNA's observed by polarized light microscopy in the columnar hexagonal liquid crystalline phase [20,26] and the DNA probed by small angle X-ray scattering in bacteriophage T4-phage heads [27]. The chains in oligonucleotide crystals and stretched fibers, however, are somewhat closer together, with interhelical separations of ~ 20 Å and intermolecular contacts between phosphorus atoms as small as ~ 6 Å [28,29].

The observed packing of DNA in crystal structures is somehow related to the chain length and conformation of the ordered strands. Most of the right-handed B-DNA dodecamer structures, for example, crystallize in the $P2_12_12_1$ space group, aligning in long columns with terminal base pairs of successive helices overlapped and with neighboring multi-helix columns vertically displaced by roughly a half molecule stagger [28]. The mode of packing, however, is not a requirement of the space group. B-DNA decamers crystallized in the monoclinic C2 and the orthorhombic $P2_12_12_1$ space groups, on the other hand, simply stack end-on-end with no terminal base overlap and a small (one to three residue) stagger between laterally flanking neighbors [29–32]. Alternate chain conformations, however, pack in totally different ways. The relatively minor opening of the central base pairs in the B-type d(ACCGGCGCCACA)·(TGGCCGCGGTGT) duplex, for example, introduces a novel packing scheme with neighboring helices locked through groove-backbone contacts in a crossed configuration [33]. Duplexes in the B-type d(CGCGAAATTT*A*CGCG)$_2$ crystal structure with unpaired adenine bases (noted in the preceding formula by italics) are also reported to associate in crossed orientations in the vicinity of the base insertions [34]. The unpaired bases in the d(CGC*A*GAATTCGCG)$_2$ B-DNA tridecamer, however, sandwich between nucleotides in a neighboring double helix, forming endless columns of parallel pseudo helices with duplex fragments aligned in alternating directions [35,36].

The even more drastic change of conformation found in A-DNA octamers leads to the association of terminal base pairs of one chain with the shallow minor groove of a neighboring duplex [37–39]. This local interaction supports several different overall packing motifs, including a cyclic sixfold spiral (space group $P6_1$), a tetragonal lattice (space group $P4_32_12$), and a threefold pattern of near neighbor contacts (space group $P3_221$), all with large solvent channels. Like B-DNA, A-DNA is a right-handed structure, but different from the former in terms of the displacement and inclination of base pairs with respect to the helical axis as well as in terms of the shapes of the grooves formed by the edges of the base pairs and the atoms of the complementary sugar-phosphate backbones [40]. Interestingly, the Z-DNA helix packs like B-DNA in long polymer-like columns. Chain ends stack in a simple end-over-end fashion and lateral strands adopt hexagonal closest packing [41] with a three-residue end overlap [42]. Unlike A- and B-DNA, Z-DNA is a left-handed helix with concave and convex grooves. In A- and B-DNA the so-called major and minor grooves are both concave, the differences in the grooves involving their relative widths and depths.

Information on the molecular packing of DNA helices available from X-ray diffraction studies of oriented fibers [43–45] is consistent with the information found in single crystal studies. The idealized A- and B-form double helical models are packed with chains in the respective unit cells parallel to one another and pointing in the same direction. Neighboring A-DNA helices are slipped

vertically by 22 Å (i.e., approximately eight base pairs) with respect to one another [46]. Neighboring B-DNA helices, in contrast, are positioned in two different ways. Some of the B-DNA duplexes are separated simply by a lateral translation (~ 23 Å), while others are translated both vertically (~ 11 Å) and laterally (~ 19 Å) [43]. The closer packing in the latter cases is apparently facilitated by the interdigitation of the grooves of the staggered duplex neighbors.

The above cited intermolecular associations are thought to reflect non-covalent forces involving the atoms of neighboring DNA's as well as those of associated solvent molecules. Such forces are known to produce characteristic pairwise atomic separations [47,48]. Tables of the nonbonded intramolecular distances commonly observed in X-ray crystallographic investigations have been previously compiled and the normal lower limits of atomic separation determined [49,50]. The shortest pairwise contacts are useful measures of the sterically allowed arrangements of a molecule. When introduced in calculations, these values provide the same measure of molecular space as the rigid spherical atomic radii of a space-filling model. In the past, these so-called Ramachandran limits have been used to explore the allowed conformations generated by the internal rotations about single bonds in isolated molecules [49–51].

In this paper we outline a new application of the Ramachandran contact criteria as a first step to understanding the higher order organization of condensed DNA. We assume that the nonbonded limits used in earlier treatments of intramolecular interactions are transferrable to the study of intermolecular interactions. We then apply these hard-sphere limits to different modes of intermolecular association in DNA–DNA helical complexes. Our approach is reminiscent of that taken

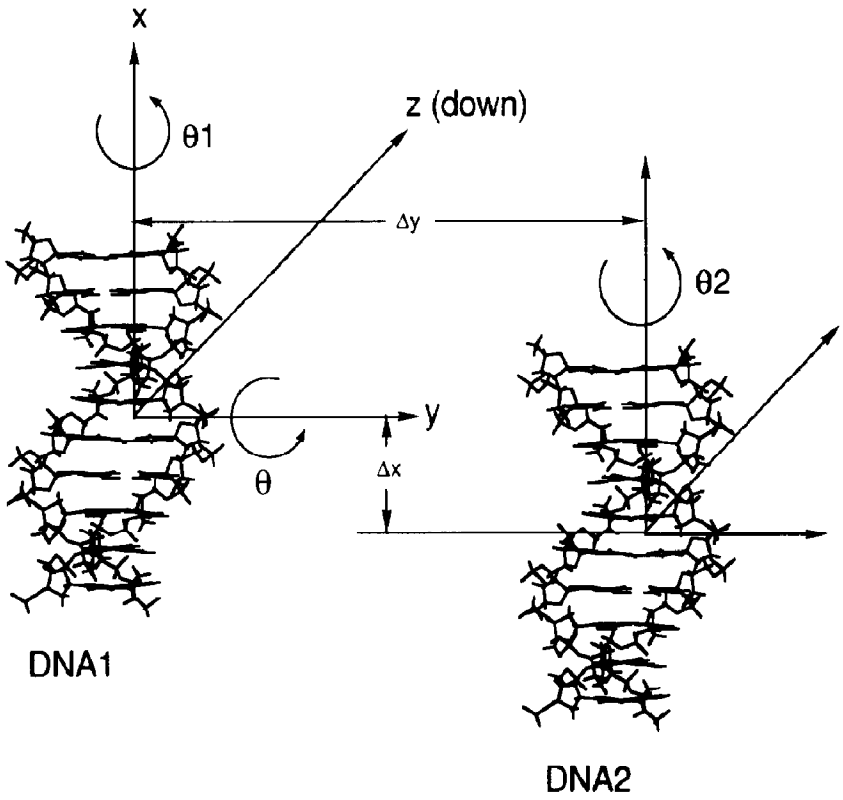

Fig. 1. Rotational (θ, $\theta 1$, $\theta 2$) and translational (Δx, Δy) parameters used to define the relative position and orientation of two B-DNA duplexes (DNA1, DNA2).

some years ago by Mazanov and Mokul'skii [52] in a study of the closest packing of B-DNA helices. In contrast to our hard-sphere approach, they computed the van der Waals' interactions between atoms in neighboring chains. They considered arrangements of parallel packed chains only and, because of the number of nonbonded interactions involved, they limited their calculations to the atoms of the sugar-phosphate backbones. Here, we consider regular double helical structures of one complete turn in A-, B-, and Z-helical forms in a variety of possible mutual spatial configurations. We accept only those arrangements of the two DNA's that are free of short interatomic contacts. As a first approximation, we ignore the presence of intervening small solvent molecules and any specific conformational perturbations of the DNA that might elicit or accompany chain packaging [53,54]. We extend our studies in selected cases to longer DNA's containing two complete helical turns. We find the computed contact-free configurations to agree surprisingly well with the packing arrangements of DNA in crystals of short oligonucleotide fragments and in stretched fibers. In addition, we observe structural features which may be relevant to the folding of DNA chains in supramolecular assemblies as well as to the long-range intramolecular interactions of DNA supercoils and cruciforms.

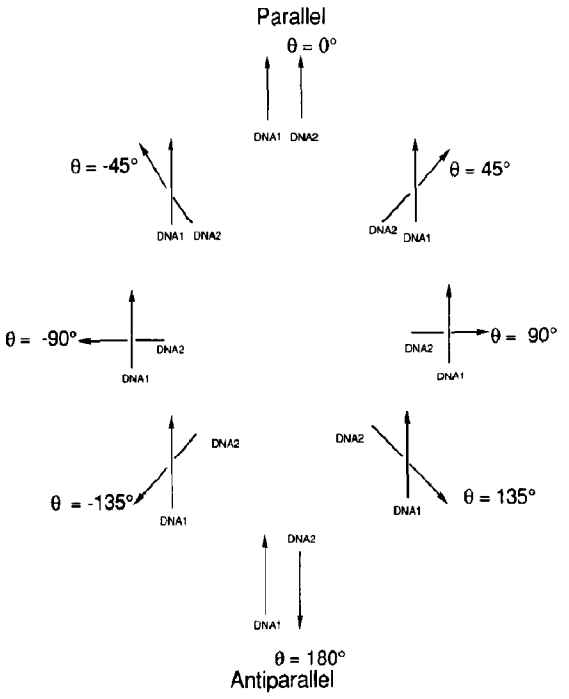

Fig. 2. Schematic illustration of the different azimuthal orientations of adjacent DNA duplexes considered in this study. For reasons of clarity in distinguishing the angles, the displacement of duplex pairs is not uniform in the figure.

2. Methods

In principle, two neighboring DNA molecules can assume a variety of mutual orientations and translations. In the present study we employ a systematic procedure involving two translational and three rotational parameters to position one DNA duplex with respect to another. The relative displacement and orientation of the two chains (referred to here as DNA1 and DNA2) of identical primary and secondary structure are described in Fig. 1. DNA1 is taken in one of the three standard double helical conformations (A, B, Z) with its helical axis directed along the x-axis of the coordinate system. The origin of the reference frame is located at the approximate geometric center of DNA1. The y-axis is chosen to pass through one of the phosphorus atoms of the duplex and the z-axis is constructed to complete a right-handed coordinate frame. The atoms of DNA2 are then generated from those of DNA1 by translations Δx (along the helix axis) and Δy (between the helical axes of the two molecules) and rotation θ (about the y-axis). The latter parameter was not considered in the earlier work by Mazanov and Mokul'skii [52]. The coordinate $\boldsymbol{x}_i'$ of atom i in DNA2 is related to the coordinate $\boldsymbol{x}_i$ of the corresponding atom in DNA1 by the following transformation:

$$\boldsymbol{x}_i' = \begin{bmatrix} \cos\theta & 0 & \sin\theta \\ 0 & 1 & 0 \\ -\sin\theta & 0 & \cos\theta \end{bmatrix} \boldsymbol{x}_i + \begin{bmatrix} \Delta x \\ \Delta y \\ 0 \end{bmatrix} \qquad (1)$$

The rotation θ-positions DNA2 with respect to DNA1 in the specified azimuthal orientation. The orientations of the DNA's considered in this study ($\theta = 0°$, $\pm 45°$, $\pm 90°$, $\pm 135°$, $180°$) are illustrated

Table 1

Minimum hard-sphere contact distances between specific atom pairs in the polynucleotide chain [49,50]

Atom pair	Contact distance (Å)
C···C	3.2
C···N	2.9
C···O	2.8
C···P	3.4
C···H	2.4
N···N	2.7
N···O	2.7
N···P	3.2
N···H	2.4
O···O	2.7
O···P	3.2
O···H	2.4
P···P	3.5
P···H	2.65
H···H	2.0

schematically in Fig. 2. The DNA1 and DNA2 are represented by their respective helical axis vectors in the figure. The relative helical slippage of the duplexes, Δx, is assigned values of 0, ± 6.8, ± 17 Å, corresponding respectively to chain ends perfectly in register, shifted vertically by two base pairs, or displaced by a half helical turn (in the case of B-DNA). The separation distance between helical axes, Δy, is varied from 17 to 19 Å at intervals of 0.5 Å. Other values of Δx and Δy are introduced for special cases reported in the text. The parameters $\theta 1$ and $\theta 2$, illustrated in Fig. 1, are rotations about the helical axes of DNA1 and DNA2, respectively. These rotations bring different parts of the double helical surfaces into direct contact. For each combination of Δx, Δy, and θ, the $\theta 1$ and $\theta 2$ molecular screw rotations are varied from 0° to 360° at 30°-intervals.

In order to assess the stereochemical acceptability of a particular helix–helix association, we apply the hard-sphere contact criteria listed in Table 1 to all atom pairs of DNA1 and DNA2. These limits correspond to the normal minimum contact distances found by Ramachandran and co-workers from surveys of the nonbonded interatomic distances in high resolution crystal structures [49,50]. We compare the interatomic separations between all the nonbonded atom pairs in DNA1 and DNA2 with these limits and tabulate the total number of contacts that violate the limits in each packing arrangement. To save computer time, we terminate the contact count if 25 such violations are found. We display the resulting number of unfavorable contacts on a steric map as a function of $\theta 1$ and $\theta 2$. Locations of zero contacts on the grid represent sterically acceptable orientations of the DNA pairs. Higher numbers indicate increased steric hindrance between adjacent DNA's. Contact numbers greater than 25 characterize highly unfavorable spatial arrangements. We present several such $\theta 1$, $\theta 2$ contact maps and the associated three-dimensional packing patterns in the following sections.

3. Results and discussion

3.1 B-DNA

3.1.1 Parallel packing of $dG_{10} \cdot dC_{10}$ B-DNA helices

The nonbonded contacts between atoms in single helical turns of two $dG_{10} \cdot dC_{10}$ oligomers, expressed in the standard B-DNA double helical conformation [45], have been assessed with the methods described above. The respective contact maps, corresponding to the B-DNA pairs positioned in parallel with $\theta = 0°$, $\Delta x = \pm 17$ Å, $\Delta y = 17$ Å, are detailed in Table 2. The numbers of short contacts corresponding to different $\theta 1, \theta 2$ combinations of molecular rotations are reported in the specified rows and columns. As seen from the grids, there is one contact-free orientation of the two DNA's (with zero forbidden contacts) at $\theta 1$, $\theta 2 = (0°, 30°)$ for $\Delta x = 17$ Å and another at $\theta 1$, $\theta 2 = (-150°, 180°)$ for $\Delta x = -17$ Å. In both cases the two B-DNA strands are staggered by a half helical turn. When the axial displacement (Δx) of the two helices is zero, there are no arrangements of the two chains with less than 25 steric contacts. For this reason, the $\Delta x = 0$ Å hard-sphere data are not tabulated here. Contact-free sites are found, however, at $\Delta x = 0$ Å if Δy is increased from 17 Å to values of 20 Å or more (data not shown).

Table 2

$\theta 1$, $\theta 2$ contact map describing allowed spatial arrangements of parallel $dG_{10}\cdot dC_{10}$ B-DNA duplexes

$\Delta x = 17$ Å, $\Delta y = 17$ Å, $\theta = 0°$														
	0	25	0^F	6	3	4^D	25	25	25	2^I	13	25	25	25
	−30	25	5	1^E	3^C	25	25	25	25	25	25	25	25	25
	−60	25	2	3^B	24	25	25	25	25	25	25	25	25	25
	−90	15	3^A	25	25	25	25	25	25	25	25	25	25	15
	−120	14	25	25	25	25	25	25	25	25	25	25	25	14
↑	−150	25	25	25	25	25	25	25	25	25	25	25	25	25
$\theta 1$(°)	180	25	25	25	25	25	25	25	25	25	25	25	25	25
	150	25	2^N	25	25	25	25	25	25	25	25	25	25	25
	120	4^M	13	25	25	25	25	25	25	25	25	25	25	4^M
	90	18	25	25	25	25	25	25	25	25	25	25	2^L	18
	60	23	25	25	25	25	25	25	25	25	25	2^K	5^H	23
	30	6^G	25	25	25	14	14	25	25	25	4^J	18	24	6^G
	0	25	0^F	6	3	4^D	25	25	25	2^I	13	25	25	25
		0	30	60	90	120	150	180	−150	−120	−90	−60	−30	0
$\theta 2$(°) →														
$\Delta x = -17$ Å, $\Delta y = 17$ Å, $\theta = 0°$														
	0	25	25	25	25	25	25	25	25	25	25	25	25	25
	−30	25	25	25	25	25	25	25	14	25	25	25	25	25
	-60	25	25	25	25	25	25	4^D	14	25	25	25	25	25
	-90	25	25	25	25	24	3^C	3	25	25	25	25	25	25
	-120	25	25	25	25	3^B	1^E	6	25	25	25	25	25	25
↑	−150	25	25	25	3^A	2	5	0^F	25	25	25	13	2^N	25
$\theta 1$(°)	180	25	25	14	15	25	25	25	6^G	23	18	4^M	25	25
	150	25	25	25	25	25	25	25	24	5^H	2^L	25	25	25
	120	25	25	25	25	25	25	25	18	2^K	25	25	25	25
	90	25	25	25	25	25	25	13	4^J	25	25	25	25	25
	60	25	25	25	25	25	25	2^I	25	25	25	25	25	25
	30	25	25	25	25	25	25	25	25	25	25	25	25	25
	0	25	25	25	25	25	25	25	25	25	25	25	25	25
		0	30	60	90	120	150	180	−150	−120	−90	−60	−30	0
$\theta 2$(°) →														

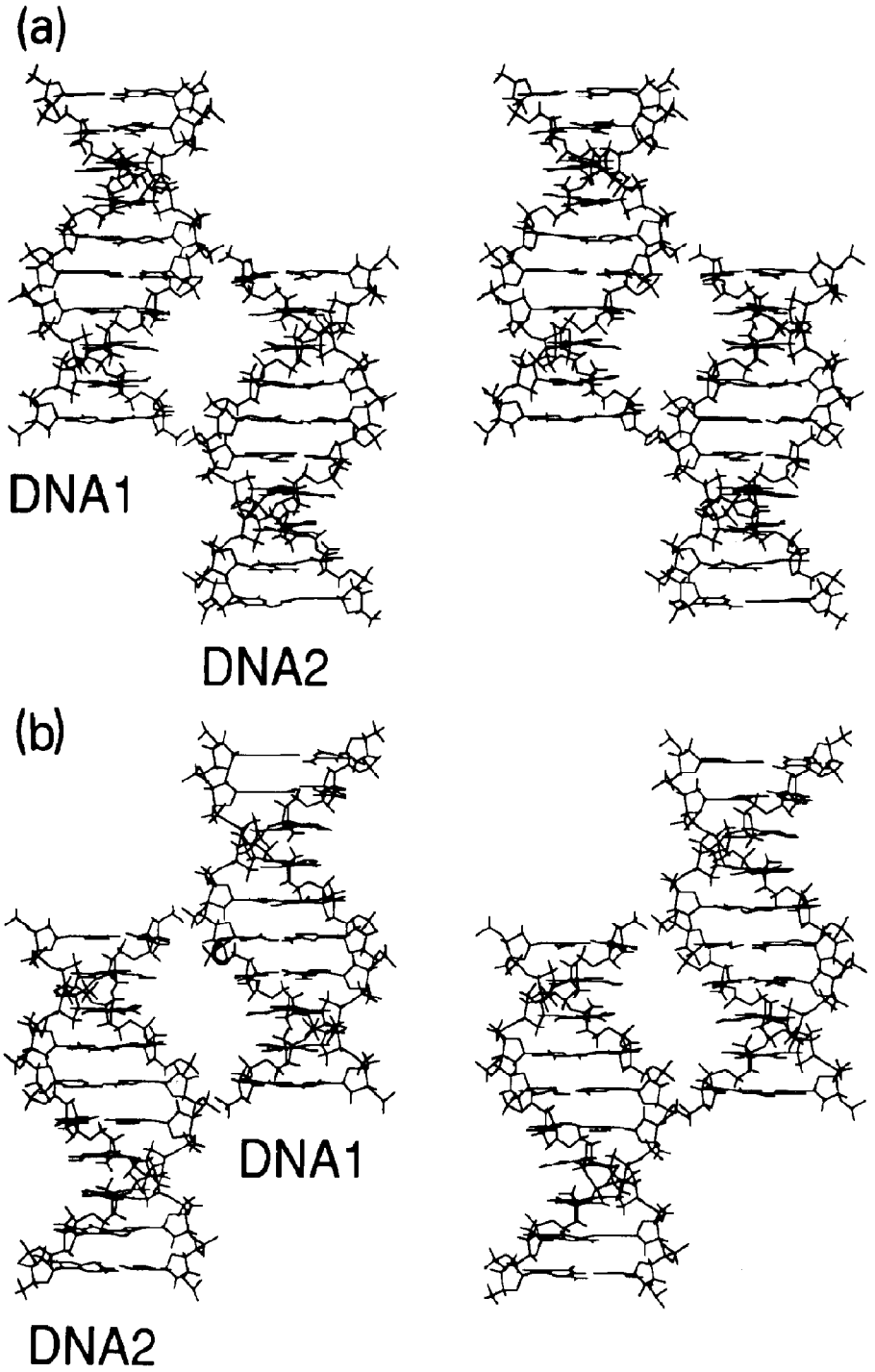

Fig. 3. Stereo representation of neighboring B-DNA $dG_{10}\cdot dC_{10}$ duplexes in the $\Delta x = -17$ Å, $\Delta y = 17$ Å, $\theta = 0°$, $\theta 1$, $\theta 2 = (-150°, 180°)$ contact-free configuration (F) from the lower half of Table 2. (a) "Front" view seen by looking in the positive z-direction; (b). "Back" view seen by looking in the negative z-direction. See to Fig. 1 for details of parameters.

It is noted that the contact maps corresponding to $\Delta x = \pm 17$ Å in Table 2 are related by symmetry. The total number of short contacts corresponding to a $\theta 1$, $\theta 2$ combination in one map is equivalent to the number of contacts corresponding to a $\theta 1'$, $\theta 2'$ arrangement in the other grid, where $\theta 1' = \theta 2 + 180°$ and $\theta 2' = \theta 1 + 180°$. Similar symmetry relationships are expected for other steric maps generated with vertical displacements Δx of equal magnitude but differing in sign, as long as the helical axes of the adjacent duplexes remain parallel (i.e., $\theta = 0°$).

Front and back views of neighboring B-DNA pairs, which adopt the short contact-free arrangement identified in Table 2, are illustrated in stereo in Fig. 3. The configuration is generated using the $\Delta x = -17$ Å, $\Delta y = 17$ Å, $\theta = 0°$, $\theta 1$, $\theta 2 = (-150°, 180°)$ parameter set. The "front" view of the B-DNA pair (seen by looking along the positive z-axis of the complex) is shown at the top of the figure and the "back" view (seen by looking in the negative z-direction) at the bottom. Two points of close contact involving the G · · · G and C · · · C sugar–phosphate backbones of neighboring molecules are apparent in both views. The distances between negatively charged phosphate groups on the two duplexes are as close as 9.4 Å in this arrangement. Different features of the DNA pair are emphasized in the two views. Particularly notable from the front view in Fig. 3(a) is the vertical stagger of the minor grooves in the complex. More interesting, however, is the "super" major groove found on the other side of the complex and illustrated in Fig. 3(b). The

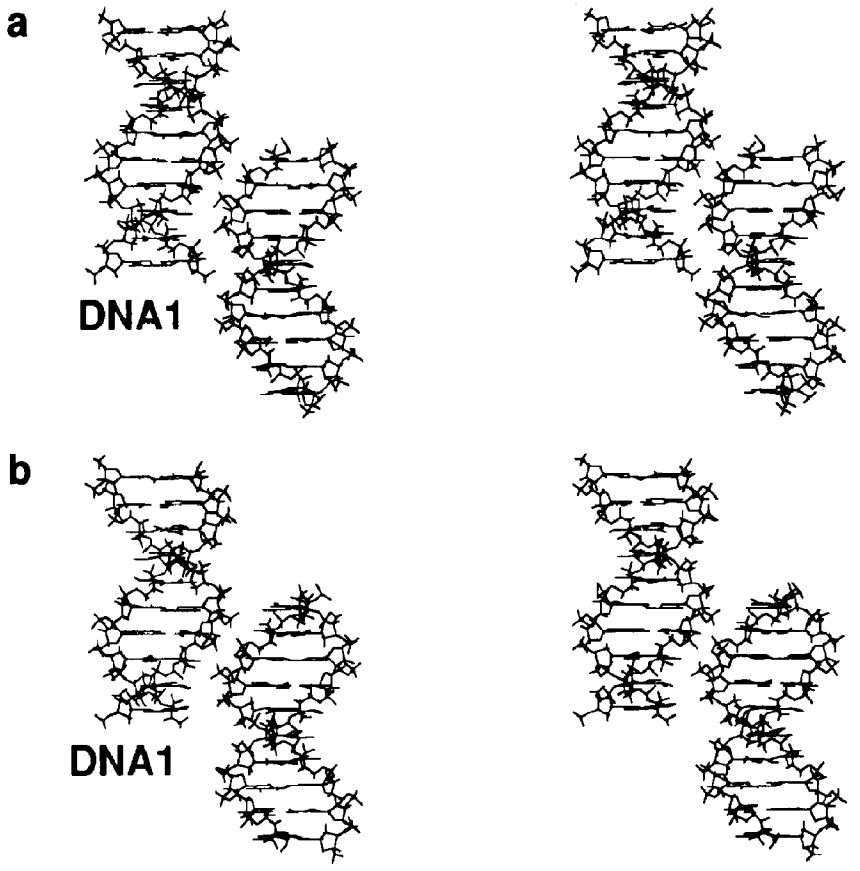

Fig. 4. Stereo representations of near contact-free packing arrangements of 10-residue B-DNA duplex pairs with $\Delta x = -17$ Å, $\Delta y = 17$ Å, $\theta = 0°$, and rotational orientations: (a) $\theta 1$, $\theta 2 = (-150°, 90°)$; (b) $\theta 1$, $\theta 2 = (-120°, 120°)$; (c) $\theta 1$, $\theta 2 = (-90°, 150°)$; (d) $\theta 1$, $\theta 2 = (-60°, 180°)$. Structures are "front" views corresponding to states *A-B-C-D* in the lower half of Table 2.

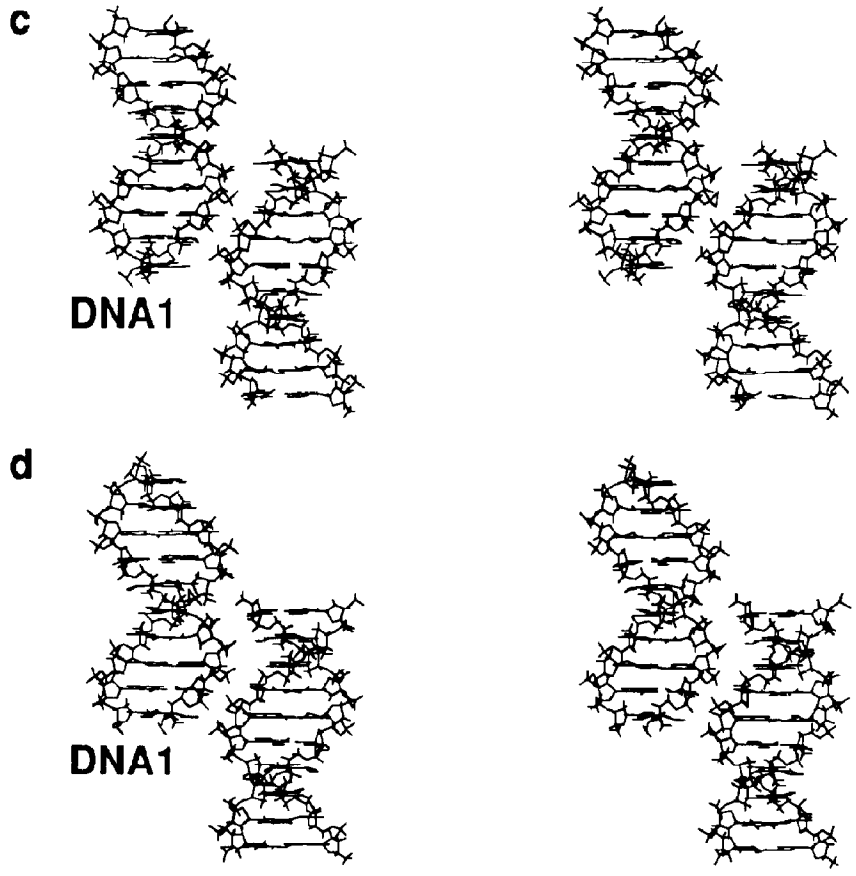

Fig. 4. (continued).

major grooves of the two DNA's are seen to run into each other in this view. Closer approach of the major grooves, however, is prevented by the backbone interactions noted above. As described below, the size and shape of the apparent "super" major groove can be fine tuned by altering the relative positions of the two duplexes. The "front" and "back" views of the packing patterns generated in the symmetrically related B-DNA pair (not shown) with $\Delta x = 17$ Å, $\Delta y = 17$ Å, $\theta = 0°$, $\theta 1$, $\theta 2 = (0°, 30°)$ are identical to those in Fig. 3, confirming the identity of the two arrangements.

The $\theta 1$, $\theta 2$ combinations of helical orientations characterized by six or fewer short contacts are highlighted in boldface and italics in Table 2. Of special interest are three sets of neighboring $\theta 1$, $\theta 2$ configurations, denoted by literal superscripts, found along different diagonals in the table. Two of the sets, *A-B-C-D* and *I-J-K-L-M-N*, are located along diagonals of positive slope in the grids, while one set, *E-F-G-H*, is found along a diagonal of negative slope. In addition, the *E-F-G-H* sequence is a pathway connecting the *A-B-C-D* and *I-J-K-L-M-N* arrangements. Packing diagrams generated by the three configurational sequences are illustrated in stereo in Figs. 4–6. The *A-B-C-D* sequence represented in Fig. 4 is characterized by close contacts between the backbones of the C-strand of DNA1 and the G-strand of DNA2. The minor grooves of the DNA's in these complexes are adjacent to one another, generating a uniform morphological pattern in the configurational sequence. The packing morphology is also uniform in the *J-K-L-M* complexes, although different from that in the *A-B-C-D* series. As illustrated in Fig. 6, the minor

grooves of the DNA's in the *J-K-L-M* series are quite far apart. There are also common backbone contacts involving the G-strand of DNA1 and the C-strand of DNA2 in the *J-K-L-M* series. Additional contacts involving either the G · · · G or C · · · C strands of the interacting DNA's are found in the packing arrangements at the ends of the *I-J-K-L-M-N* series. In contrast to the *A-B-C-D* and *I-J-K-L-M-N* configurational series, the packing morphology and the sugar–phosphate backbone contacts are altered at each step along the *E-F-G-H* sequence (Fig. 5). The zero-contact packing arrangement (e.g., *F* in Fig. 5b) noted above with a "super" major groove (Table 2 and Fig. 3) is located midway along the $\theta 1$, $\theta 2$ transition between the *A-B-C-D* adjacent minor groove structures and the *I-J-K-L-M-N* distant minor groove configurations.

3.1.2 Parallel packing of $dG_{20} \cdot dC_{20}$ B-DNA helices

In order to understand the packing motifs of B-DNA at the polymeric level, the hard-sphere calculations have been extended to $dG_{20} \cdot dC_{20}$ duplex pairs with two complete helical turns. The helical axes of the two DNA's are fixed in a parallel ($\theta = 0°$) orientation with the vertical slippage Δx set at 0 Å or ±17 Å (i.e. , perfectly aligned or displaced up or down by a half helical turn, respectively). The interhelical separation

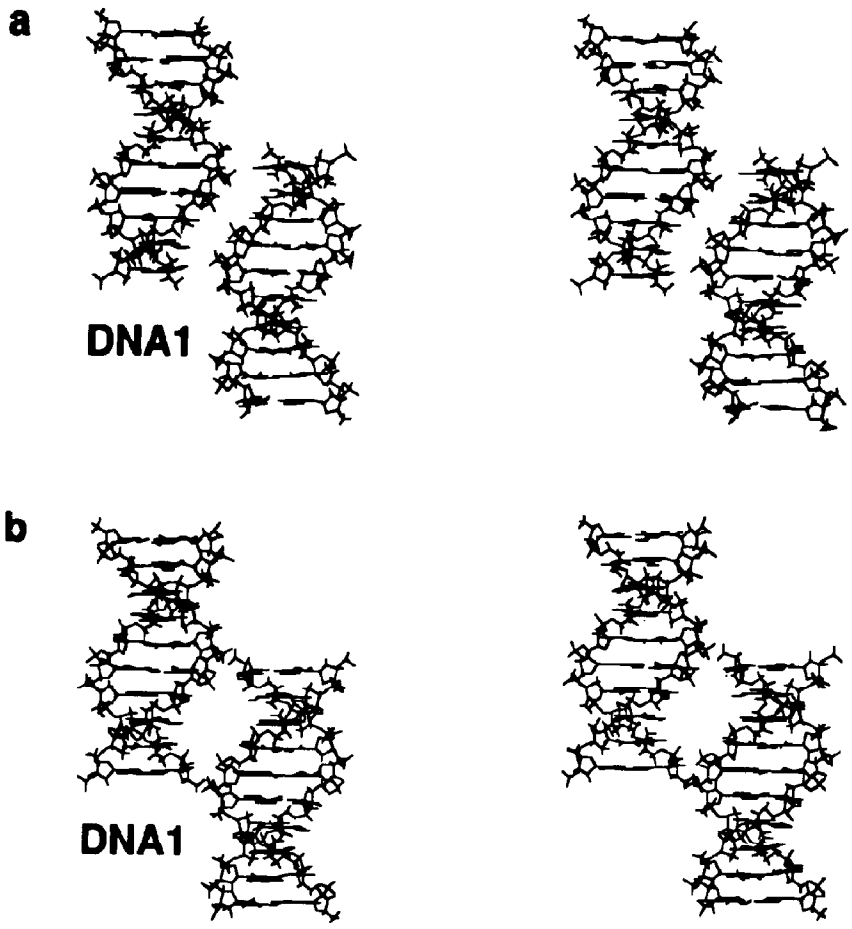

Fig. 5. Stereo representations of near contact-free packing arrangements of 10-residue B-DNA duplex pairs with $\Delta x = -17$ Å, $\Delta y = 17$ Å, $\theta = 0°$, and rotational orientations: (a) $\theta 1$, $\theta 2 = (-120°, 150°)$; (b) $\theta 1$, $\theta 2 = (-150°, 180°)$; (c) $\theta 1$, $\theta 2 = (180°, -150°)$; (d) $\theta 1$, $\theta 2 = (150°, -120°)$. Structures are "front" views corresponding to states *E-F-G-H* in the lower half of Table 2.

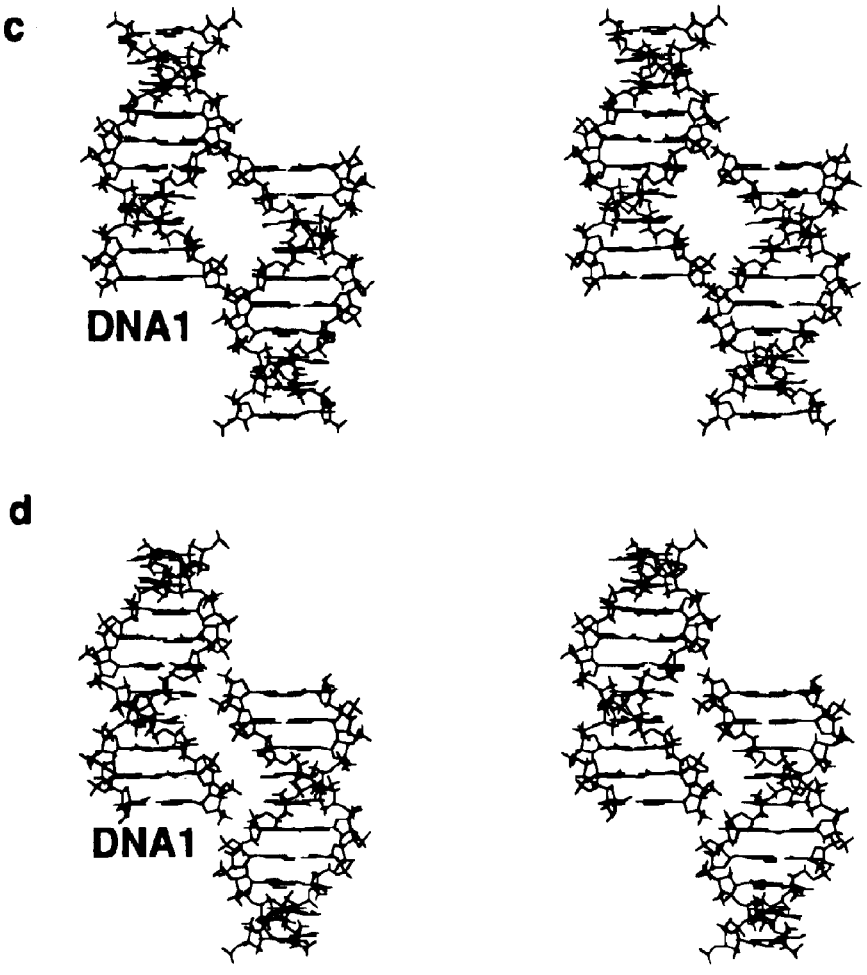

Fig. 5. (continued).

Δy, however, is increased over the values adopted in the study of $dG_{10} \cdot dC_{10}$, the parameter ranging between 18 Å and 22 Å at increments of 1 Å. The larger distances are required to relieve the steric conflicts that arise in the packing of longer helical strands. The contact map, generated by positioning the 20-residue B-DNA pairs in a slipped packing arrangement where $\Delta x = -17$ Å, $\Delta y =$ 20.5 Å, $\theta = 0°$ is presented in Table 3. Numerous contact-free or near contact-free $\theta 1$, $\theta 2$ states are apparent from the map. Indeed, there are several correlated configurational pathways linking the contact-free states. The $\theta 1$, $\theta 2$ states with six contacts or less are highlighted in boldface and italics in the table. The allowed values are found along diagonals on the grid where the difference $\theta 1 - \theta 2$ is a constant. As discussed in more detail below, $\theta 1 - \theta 2$ is a useful index to interpret the packing data in terms of crystallographic symmetry groups. An assembly of chains packed in pairs at $\theta 1 - \theta 2$ angles of $\pm 60°$, $\pm 90°$, $\pm 120°$, and $\pm 180°$ corresponds respectively to the hexagonal, tetragonal, trigonal, and orthorhombic/monoclinic crystallographic symmetry groups. (These symmetry groups are also related to the identical values of the interhelical rotation angle θ.) The correlated contact-free combinations of $\theta 1$ and $\theta 2$ observed in the hard-sphere calculations lie within a very narrow range of interhelical separation distances ($\Delta y = 21 \pm 0.5$ Å). At

shorter values of Δy there are no sterically allowed packing arrangements and at larger distances every $\theta 1$, $\theta 2$ configuration is contact-free.

The packing patterns associated with many of the allowed $\theta 1$, $\theta 2$ arrangements in Table 3 also appear to fit into a common motif. A stereo pair corresponding to one such combination where $\theta 1$, $\theta 2 = (150°, 60°)$, is illustrated in Fig. 7. The "front" view of the 20-residue pair, as defined above, is shown at the top of the figure and the "back" view at the bottom. Close interactions between the G-strand of DNA1 and the C-strand of DNA2 are evident in these representations. The formation of a "super" major groove structure is also apparent from the "back" (e.g., bottom) view of the pair. This "super" groove, however, is somewhat more offset than that observed for the decamer pair in Fig. 3 owing to the different backbone contacts in the two systems. There is only one point of close approach per helical turn in the 20-mer pairs in Fig. 7 but two such points per turn in the decamer pairs in Fig. 3. Because of this difference, the minor grooves of the packed 20-mers in Fig. 7 are interdigitated and do not form an ideal continuous extended groove. Similar long-range organizational motifs

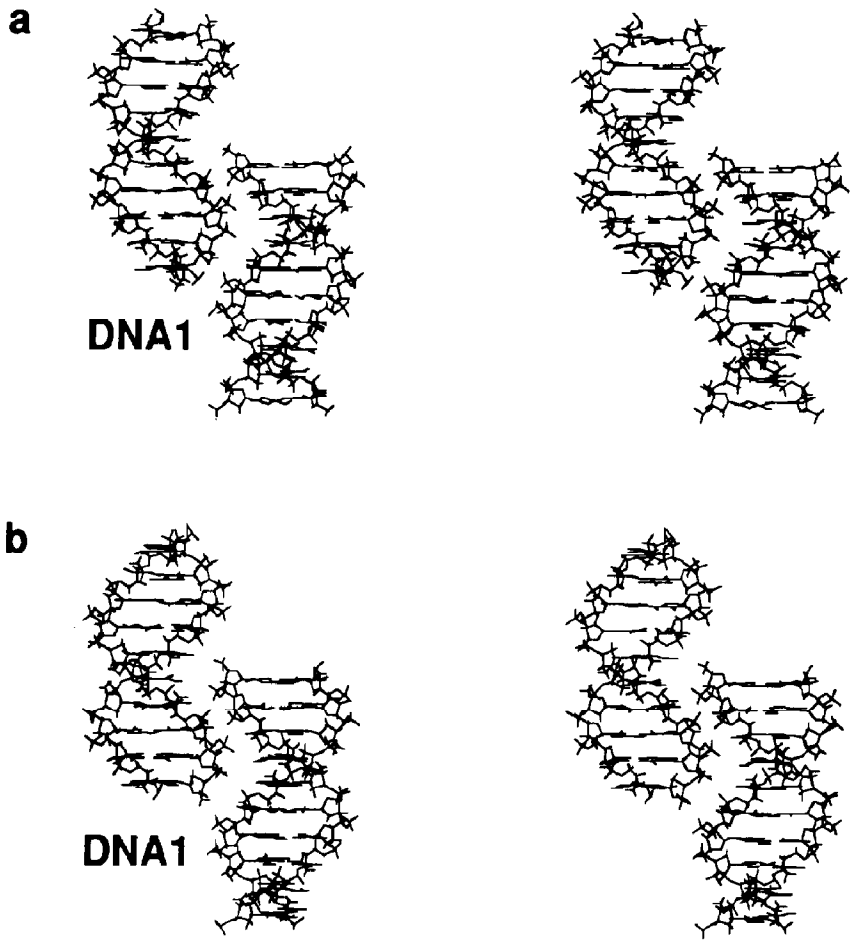

Fig. 6. Stereo representations of near contact-free packing arrangements of 10-residue B-DNA duplex pairs with $\Delta x = -17$ Å, $\Delta y = 17$ Å, $\theta = 0°$, and rotational orientations: (a) $\theta 1$, $\theta 2 = (90°, -150°)$; (b) $\theta 1$, $\theta 2 = (120°, -120°)$; (c) $\theta 1$, $\theta 2$a $(150°, -90°)$; (d) $\theta 1$, $\theta 2 = (180°, -60°)$. Structures are "front" views corresponding to states J-K-L-M in the lower half of Table 2.

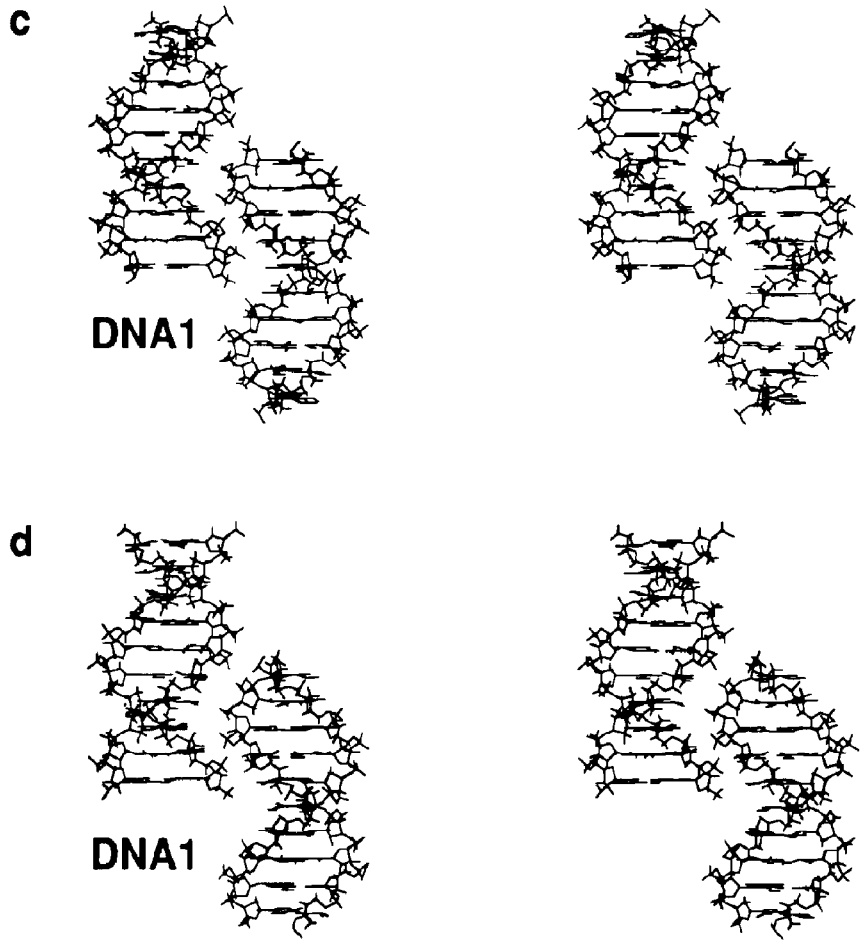

Fig. 6. (continued).

are observed when the interacting DNA's are packed in an antiparallel fashion with helical axes running in opposing directions (i.e., $\theta = 180°$).

The recently reported crystal structures of the $d(CCAACGTTGG)_2$ and $d(CGATCGATCG)_2$ B-DNA decamers in monoclinic and orthorhombic unit cells, respectively [29,31,32], present packing patterns that are quite similar to the parallel packing motif of $dG_{20} \cdot dC_{20}$ duplex pairs illustrated in Fig. 7. Endless columns of stacked helices are found to be packed side-by-side in these crystals with the phosphate groups of individual chains interlocked in the minor grooves of their immediate neighbors. Moreover, the strands in both the monoclinic and orthorhombic crystal structures are packed in square arrays, consistent with the 90° rotational differences between $\theta 1$ and $\theta 2$ in the theoretical model. As illustrated in Fig. 8, a repeating sequence of B-DNA 20-mer pairs related by $\theta 1$, $\theta 2 = (150°, 60°)$ angles generates a comparable superstructure with duplexes arranged in squares and perfectly stacked above one another in long pseudo polymeric columns. The interdigitated "super" groove apparent in Figs. 7 and 8 is also evident in the crystal structures of the B-DNA decamers, the slippage apparently assisting a good fit in the packing. Adjacent helices in the crystal complexes, however, are vertically displaced less than those in the computational model (i.e., 7–10 Å, or roughly

Table 3

$\theta 1$, $\theta 2$ Contact map describing allowed spatial arrangements of parallel $dG_{20} \cdot dC_{20}$ B-DNA duplexes

$\Delta x = -17$ Å, $\Delta y = 20.5$ Å, $\theta = 0°$														
	−0	25	***6***	***1***	***4***	12	13	***4***	15	8	***1***	***2***	10	25
	−30	16	***1***	***3***	12	7	8	25	14	***0***	***6***	25	25	16
	−60	***3***	***5***	10	***5***	25	14	24	***2***	9	25	14	25	***3***
	−90	***1***	12	8	25	7	24	8	***6***	25	11	25	***3***	***1***
	−120	9	13	9	15	24	***6***	***2***	16	25	25	***6***	***0***	9
↑	−150	24	***4***	25	24	***6***	***2***	12	25	22	***6***	***2***	12	24
$\theta 1$(°)	180	***4***	15	17	***2***	***4***	14	25	12	***2***	8	24	25	***4***
	150	12	7	***0***	9	25	25	20	***2***	***6***	24	14	7	12
	120	12	***1***	***6***	25	13	25	***6***	10	21	7	25	7	12
	90	***4***	***3***	25	10	25	***6***	***2***	24	16	25	***5***	12	***4***
	60	***1***	11	25	25	***3***	***0***	17	25	9	8	12	***3***	***1***
	30	***6***	25	17	***3***	***1***	7	24	***4***	13	12	***3***	***1***	***6***
	0	25	***6***	***1***	***4***	12	13	***4***	15	8	***1***	***2***	10	25
		0	30	60	90	120	150	180	−150	−120	−90	−60	−30	0
$\theta 2$(°) →														

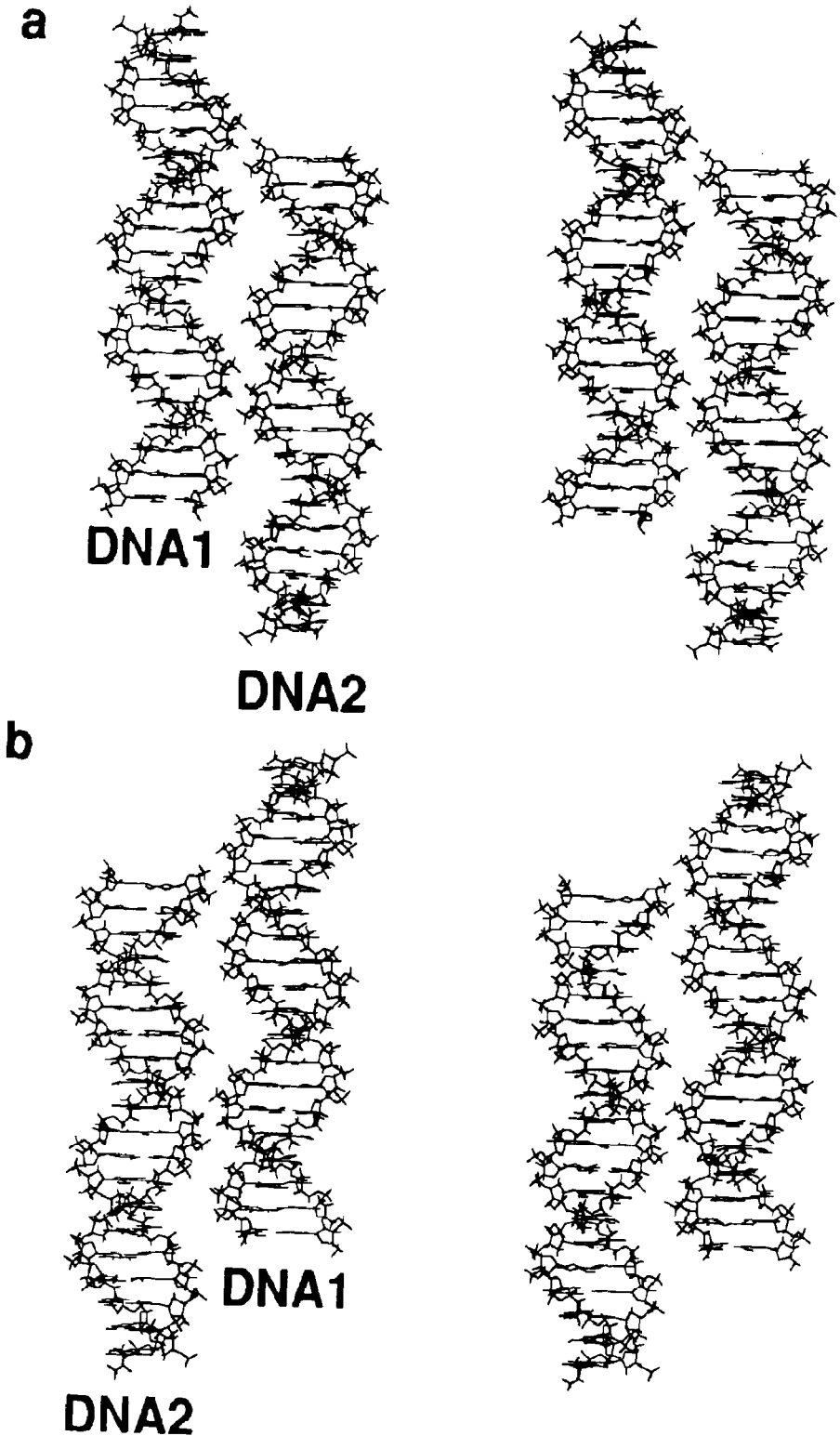

Fig. 7. Stereo representations of (a) "front" and (b) "back" views of a pair of $dG_{20} \cdot dC_{20}$ B-DNA duplexes positioned with $\Delta x = -17$ Å, $\Delta y = 20.5$ Å, $\theta = 0°$, $\theta 1$, $\theta 2 = (150°, 60°)$.

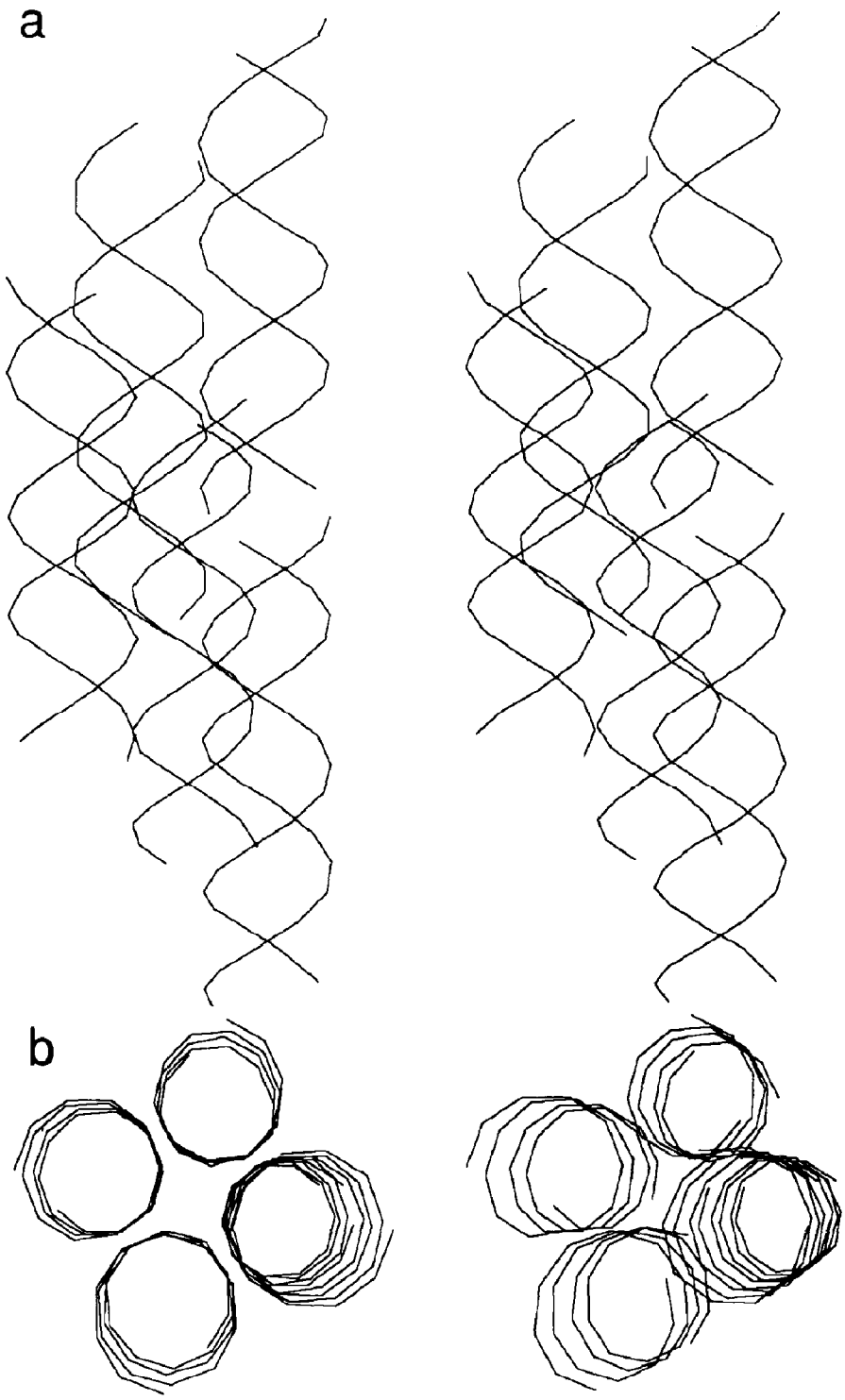

Fig. 8. Stereo views of the superstructure formed by pairwise associations of five $dG_{20}\cdot dC_{20}$ B-DNA duplexes positioned in the contact-free orientation detailed in Fig. 7 and represented at the P–P virtual bond level. (a) View perpendicular to the helix axis; (b) view projected down the helix axis.

Table 4

Number of $\theta 1$, $\theta 2$ arrangements of A-, B-, and Z-DNA helical pairs [a] with zero hard-sphere contacts

Δx, Δy (Å)	Structure	θ(°)							
		0	45	90	135	180	−135	−90	−45
+17, 17	A-DNA	14	14	29	13	14	12	30	12
	B-DNA	1	16	42	16	1	18	43	17
	Z-DNA	6	55	61	32	10	56	60	41
+6.8, 17	A-DNA	0	0	0	0	0	0	0	0
	B-DNA	0	2	10	1	0	1	10	0
	Z-DNA	2	41	57	22	2	43	57	20
0, 17	A-DNA	0	0	0	0	0	0	0	0
	B-DNA	0	0	16	0	0	1	17	0
	Z-DNA	0	41	60	28	0	42	61	20
−6.8, 17	A-DNA	0	0	0	0	0	0	0	0
	B-DNA	0	2	10	0	0	2	10	1
	Z-DNA	2	42	62	25	0	44	57	21
−17, 17	A-DNA	14	14	31	12	16	9	31	14
	B-DNA	1	18	47	19	1	20	45	16
	Z-DNA	6	50	52	34	5	52	52	30

[a] A- and B-DNA duplexes composed of 10 base pairs; Z-DNA duplexes of 12 base pairs.

2–3 base pairs, in the crystal versus 17 Å here). This is not surprising given the shorter end-to-end length of the decamers versus the 20-residue pairs in the current model. A slightly greater vertical displacement compared to the theoretical model (i.e., 22 Å per 20-mer repeat) is reported in the structure of B-DNA deduced on the basis of the diffraction of oriented fibers [43]. The strands are also more closely packed in both the decamer crystals and the B-DNA fibers than in the current model, the distances between helical centers being 19.5–19.7 Å in the decamers, 19.0 Å in the fiber model, and 20.5 Å in this study. The closer approach of adjacent chains in the X-ray structures may be facilitated by the different vertical displacements of neighboring duplexes pointed out above as well as by the irregular conformation of the sugar–phosphate backbone in the crystalline decamers versus the ideal B-DNA helical conformation adopted here.

3.1.3 General packing of $dG_{10} \cdot dC_{10}$ A-, B-, and Z-DNA helices

The total numbers of contact-free ($\theta 1$, $\theta 2$) states found in the side-by-side packing of pairs of A-, B-, and Z-DNA duplexes of one helical turn are compiled in Table 4. The data are tabulated for different mutual arrangements of the duplex pairs corresponding to vertical displacements $\Delta x = 0$, ± 6.8, ± 17 Å, interhelical spacings $\Delta y = 17$ Å, and mutual orientations $\theta = 0°$, $\pm 45°$, $\pm 90°$, $\pm 135°$, $180°$. As evident from the table, the number of contact-free configurations is a function of helix type, orientation angle (θ), and vertical displacement (Δx). Overall, the most contact-free states are associated with the 12-residue Z-DNA fragments. A total of 1,351 contact-free arrangements is found for the Z-DNA pairs versus 279 for the 10-residue A-DNA pairs and 404 for the 10-residue B-DNA pairs. It is clearly easier for the slimmer Z-DNA fragments to pack at $\Delta y = 17$ Å helical separation distances than the more shapely (in terms of groove geometry) A- and B-DNA structures. The number of contact-free arrangements for all three helical models is increased if the computations are carried out at greater interhelical separation distances (i.e., Δy 17 Å). According to Table 4, the packing of short A-, B-, and Z-DNA helical pairs, as measured by the number of zero-contact states, is best at crossed orientations where $\theta =$

± 45–$135°$. Such arrangements are closely related to the crossed packing patterns of certain DNA duplexes in the solid state (see below) as well as to the configurations of supercoiled DNA where sequentially distant parts of the polymer are in close spatial proximity [55] or to the structures of Holliday junctions where the strands of two duplexes can be interchanged [56–58]. Local crossed packing arrangements are also expected to facilitate the interactions of layers of parallel molecules in three-dimensional lattices in both liquid crystalline and solid phases [59].

3.1.4 Comparison with B-DNA dodecamer crystals

The hard-sphere B-DNA calculations have been extended to the $dG_{12} \cdot dC_{12}$ duplex pair to compare the predicted molecular packing with that observed in the $d(CGCGAATTCGCG)_2$ dodecamer crystal structure [60]. The DNA fragments are represented, for simplicity, by ideal B-type structures rather than the exact atomic coordinate set. The mutual orientations (θ) of helices are held at 180° in order to mimic the antiparallel arrangements of DNA pairs (related by 2_1 screw axis symmetry) in the crystal. The relative vertical translation between interacting helices is assigned values of $\Delta x = 0$, ± 20.4 Å, and the horizontal displacement of the helix axes values of $\Delta y = 16$, 17, 17.5, 18, 18.5 Å. The $\Delta x = 20.4$ Å vertical stagger (i.e., approximately six base pairs) is roughly equal to the vertical translation observed in the crystal structure. The

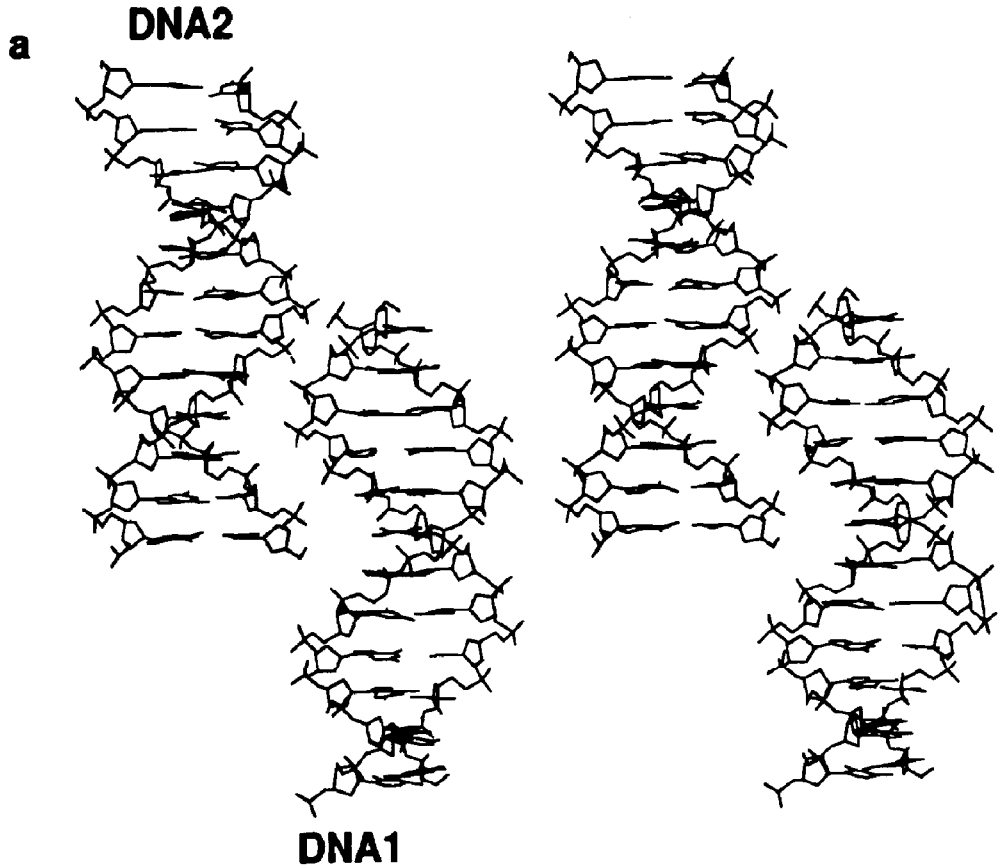

Fig. 9. Comparative stereo representations of the intermolecular packing of (a) two $dG_{12} \cdot dC_{12}$ B-DNA fragments allowed on the basis of hard-sphere contacts when $\Delta x = 20.4$ Å, $\Delta y = 17.5$ Å, $\theta = 180°$, $\theta 1$, $\theta 2 = (90°, 180°)$ and (b) two $d(CGCGAATTCGCG)_2$ molecules related by the 2_1 screw axis symmetry found in the crystal structure [60]. To facilitate comparison between structures, the hydrogen atoms used in the hard-sphere analysis are not shown.

lateral spacing of helical axes in the crystal (24 Å) [29], however, is somewhat larger than the values used here (see below).

Interestingly, there are no contact-free arrangements found when the dodecamer pair is packed with zero vertical translation and the horizontal displacement and axial rotations are varied over the ranges listed above. Several $\theta 1$, $\theta 2$ rotational combinations, however, are permitted if the chains are slipped vertically with $\Delta x = \pm 20.4$ Å. A single contact-free state at $\theta 1$, $\theta 2 = (-60°, 120°)$ is noted on the map (not shown) corresponding to $\Delta x = 20.4$ Å, $\Delta y = 17$ Å, and $\theta = 180°$ and three such arrangements at $\theta 1$, $\theta 2 = (-30°, 90°)$, $(-60°, 120°)$, and $(-90°, 150°)$ are found when the interhelical separation distance Δy is increased to 17.5 Å. There are seven other $\theta 1$, $\theta 2$ configurations, found at $(-60°, 150°)$, $(-30°, 120°)$, $(0°, -90°)$, $(30°, -90°)$, $(60°, -120°)$, $(90°, -150°)$, $(90°, 180°)$, with six or fewer short contacts on the latter grid (not shown). The "back" view of one of these low contact states where $\Delta x = 20.4$ Å, $\Delta y = 17.5$ Å, $\theta = 180°$, $\theta 1$, $\theta 2 = (90°, 180°)$ is compared in Fig. 9 with the DNA dyad observed in the d(CGCGAATTCGCG)$_2$ crystal structure. (As noted above, this contact-free configuration is related symmetrically to a second contact-free state found when the chains are displaced vertically by $\Delta x = -20.4$ Å.) The qualitative similarity between the theoretical model and the crystal packing pattern is apparent from the figure. An extended "super" major groove is evident in both the theoretical and the experimental models. The average distance between the minor groove edges in the theoretical model, however, is notably smaller

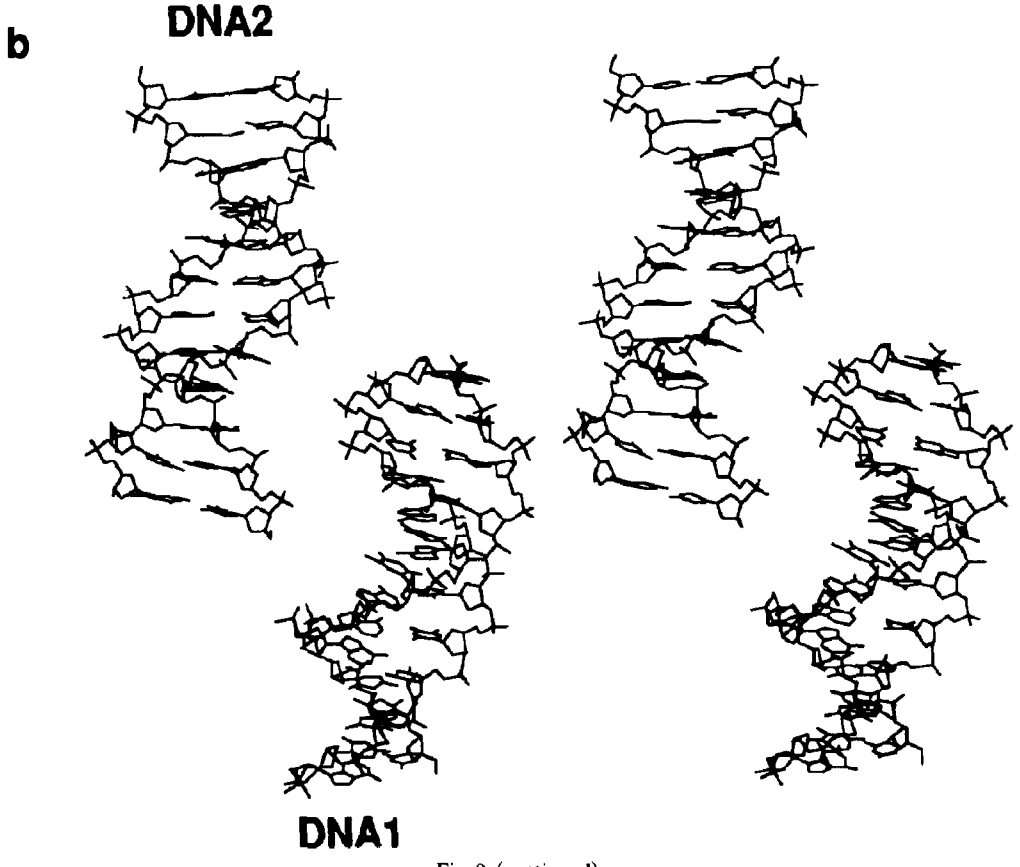

Fig. 9. (continued).

than the corresponding distance in the crystal structure (21.35 Å versus 25.82 Å). This discrepancy may be related to the geometric irregularities in the crystal structure versus the regular monomeric repeating structure in the computational model as well as to the different interhelical displacements in the X-ray and theoretical complexes. Solvent (i.e., water) molecules are interspersed between the DNA's in the crystal structure. The contact criteria applied in the current calculations, however, are not corrected to include solvent effects. The predicted intermolecular spacing would be greater if the hard-sphere contact criteria were increased in value or if the positions of solvent molecules were explicitly considered. The presence of bound water in the grooves of the dodecamer crystal is well documented [61]. In the crystal there are also strong water-mediated hydrogen bonds between neighboring helices, which are not considered here.

In addition, the sterically allowed pairwise interactions presented above cannot account for the three-dimensional molecular lattice in the dodecamer crystal. Regular repetition of adjacent dodecamer pairs in the computed low contact configuration in Fig. 9(a) produces a three-dimensional square array. While a square motif also occurs in the crystal structure, it arises from different sorts of intermolecular interactions (i.e., not close contacts of antiparallel duplexes). The interactions of antiparallel duplexes in the crystal corresponding to those in Fig. 9(b) lead to a planar sheet of molecules. A planar sheet of dodecamers resembling that found in the crystal structure, however, can be generated using the contact-free state at $\theta 1$, $\theta 2 = (-60°, 120°)$ on the $\Delta y = 17$ Å grid cited above or the low contact configuration at $\theta 1$, $\theta 2 = (60°, -120°)$ on the $\Delta y = 17.5$ Å grid. In both cases the magnitude of the difference in molecular rotational parameters $|\theta 1 - \theta 2|$ equals 180°.

As noted above, two symmetry related molecules in the d(ACCGGCGCCACA)·(TGGCCGCGGTGT) crystal structure are locked together by reciprocal groove-backbone interactions [33]. The helical axes of this DNA pair are reported to be mutually inclined at an angle of 60°. Model calculations of the contact-free packing of two twelve base pair fragments of ideal B-DNA (i.e., $dG_{12} \cdot dC_{12}$) inclined at an angle $\theta = 60°$ are found to result in a similar packing arrangement. Computations have been performed with helices inclined at this angle for all $\theta 1$, $\theta 2$ combinations with $\Delta x = 0$ Å and $\Delta y = 16$,

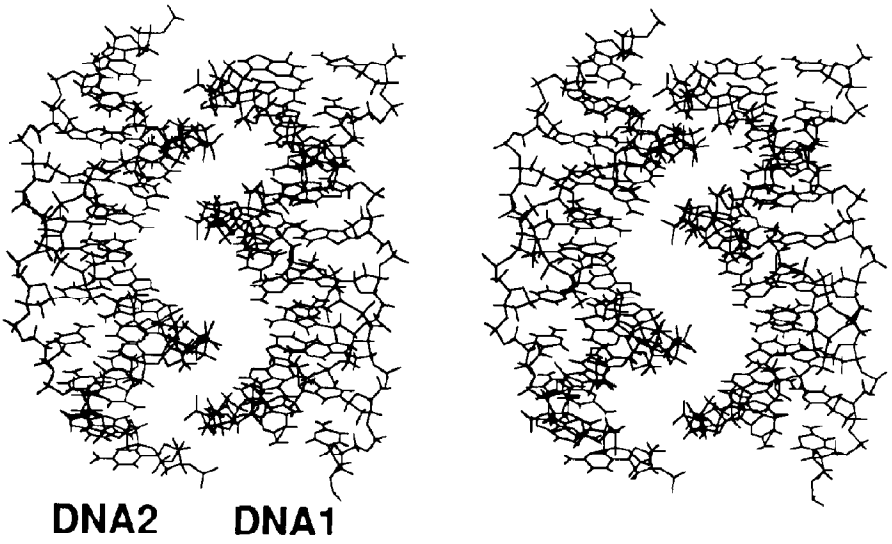

Fig. 10. Stereo representation of the predicted three-dimensional packing of two $dG_{12} \cdot dC_{12}$ B-DNA duplexes with helical axes inclined at an angle $\theta = 60°$ with $\Delta x = 0$ Å, $\Delta y = 17$ Å, $\theta 1$, $\theta 2 = (180°, -90°)$.

17, 17.5, 18, 18.5 Å. Four contact-free configurations are found in the $\Delta y = 17$ Å grid (not shown) at $\theta 1$, $\theta 2$ = (60°, −30°), (90°, 0°), (150°, −120°), and (180°, −90°). The first and the third, and the second and the fourth of these states are symmetrically related, producing identical three-dimensional packing patterns. The contact-free B-DNA complex generated with $\Delta x = 0$ Å vertical displacement, $\Delta y = 17$ Å lateral separation, $\theta = 60°$ azimuthal orientation, and $\theta 1$, $\theta 2$ = (180°, −90°) helical axis rotations is illustrated in stereo in Fig. 10. This complex is very similar on visual inspection to the X-ray crystal structure reported by Timsit et al. in Fig. 3 of their 1989 paper [33]. The phosphate backbone of one of the DNA's in Fig. 10 interacts with the bases (in the major groove) of the neighboring duplex in a fashion similar to the interactions reported in the crystal complex. The theoretical B-DNA association corresponding to $\Delta x = 0$ Å, $\Delta y = 17$ Å, $\theta = 60°$, $\theta 1$, $\theta 2$ = (150°, −120°) presents a similar pattern of interactions (not shown here). The latter complex, however, is likely to be somewhat higher in energy than the structure illustrated in Fig. 10. There are 59 nonbonded contacts in the range of 3.5–4.5 Å between the H, C, O, N, and P atoms of the DNA's in Fig. 10 (i.e., potentially favorable van der Waals interactions), but only 29 such contacts in the alternate complex which is not shown. In addition, there are roughly the same number of phosphate pairs within 10 Å of one another in the two complexes (23 and 19, respectively), suggesting that the electrostatic interactions of the two forms are comparable. It is also noted that the regular repetition of intermolecular interactions in Fig. 10 introduces a left-handed twist in a three-dimensional assembly of crossed dodecamer pairs. The overall packing motif in the d(ACCGGCGCCACA) · (TGGCCGCGGTGT) crystal, however, has not yet been fully described.

3.2 A-DNA

3.2.1 Parallel packing of $dG_{10} \cdot dC_{10}$ A-DNA helices

A contact map describing the parallel ($\theta = 0°$) packing of $dG_{10} \cdot dC_{10}$ duplexes fixed in a standard A-DNA conformation [44] is reported in Table 5. In this example the two A-DNA's are laterally displaced by $\Delta y = 17$ Å and vertically separated by $\Delta x = -17$ Å. The sterically acceptable $\theta 1$, $\theta 2$ configurations (each with six or fewer hard-sphere contacts) are highlighted in boldface and italics on the grid. It is noteworthy that 14 of these 22 states are completely free of steric contacts. This is in contrast to only a single contact-free state associated with the corresponding B-DNA duplex pair examined under the same geometric conditions (Table 2). The range of acceptable packing of parallel A-DNA decamers is thus somewhat broader than that for B-DNA decamers at the same lateral translation ($\Delta y = 17$ Å) and displacement ($\Delta x = \pm 17$ Å). This behavior is expected given the short, squat shape of A-DNA versus the thinner and more extended form of B-DNA. At $\Delta x = \pm 17$ Å (approximately half helical turns), contacts between the A-DNA's are confined primarily to chains ends (see below), whereas in B-DNA there are contact points in central parts of the duplex.

The range of A-DNA packing orientations is also spatially different from that in B-DNA. The allowed combinations of $\theta 1$ and $\theta 2$ for the A-DNA's are clustered over a broad area of the contact surface, rather than spread out along several narrow interdependent orientational pathways (compare Table 5 with Table 2). The contact grid corresponding to vertical translation $\Delta x = -17$ Å for the A-DNA's in Table 5 is related to the $\Delta x = +17$ Å grid by the same symmetry relationship described earlier for parallel B-DNA pairs and thus is not reported here. The A-DNA chains are found, like B-DNA, to self-intersect at $\Delta x = 0$ Å with no contact-free arrangements on the $\theta 1$, $\theta 2$ grid.

Five of the 14 contact-free $\theta 1$, $\theta 2$ combinations listed in Table 5 have been selected to illustrate the nature of A-DNA decamer packing in Fig. 11. These configurations where $\theta 1$, $\theta 2$ = (−150°, −60°), (120°, −120°), (−150°, −120°), (−90°, −120°), and (−150°, 180°), are denoted respectively by literal superscripts *A-E* in Table 5. "Back" views of neighboring *A*-DNA molecules packed in these arrangements are shown in stereo in the figure. The stereo pairs

Table 5

$\theta 1$, $\theta 2$ Contact map describing allowed spatial arrangements of parallel $dG_{10} \cdot dC_{10}$ A-DNA duplexes

$\Delta x = -17$ Å, $\Delta y = 17$ Å, $\theta = 0°$														
	0	25	25	25	25	25	25	25	25	25	25	25	25	25
	−30	25	25	25	25	25	25	25	25	25	25	25	25	25
	−60	25	25	25	25	25	25	25	25	***2***	25	25	25	25
	−90	25	25	25	25	25	25	21	***2***	$\boldsymbol{0}^{D}$	7	25	25	25
	−120	25	25	25	25	25	22	***3***	***0***	***0***	***0***	***3***	25	25
↑	−150	25	25	25	25	22	***4***	$\boldsymbol{0}^{E}$	***0***	$\boldsymbol{0}^{C}$	***0***	$\boldsymbol{0}^{A}$	***6***	25
$\theta 1$(°)	180	24	25	25	25	25	***6***	***0***	***0***	7	25	22	***6***	24
	150	25	25	25	25	25	25	10	***0***	***0***	25	25	25	25
	120	25	25	25	25	25	25	25	9	$\boldsymbol{0}^{B}$	25	25	25	25
	90	25	25	25	25	25	25	25	25	20	25	25	25	25
	60	25	25	25	25	25	25	25	25	25	25	25	25	25
	30	25	25	25	25	25	25	25	25	25	25	25	25	25
	0	25	25	25	25	25	25	25	25	25	25	25	25	25
		0	30	60	90	120	150	180	−150	−120	−90	−60	−30	0
$\theta 2$(°) →														

labeled *A* and *B* are aligned so that the terminal base pair of one duplex is packed against the sugar-phosphate backbone of its neighbor. The minor groove of one of the DNA's runs into the major groove of the other in these arrangements, forming an extended groove structure. The interactions in configurations *C*, *D*, and *E* are similar to those found above for 20-residue B-DNA's with neighboring backbones interacting at a single site. The major grooves of the two A-DNA duplexes in these three arrangements are also seen to run into each other forming an extended "super" groove. As detailed in a later section, similar extended "super" grooves are noted when longer A-DNA fragments (20-mers) are examined. The terminal backbone-base pair interac-

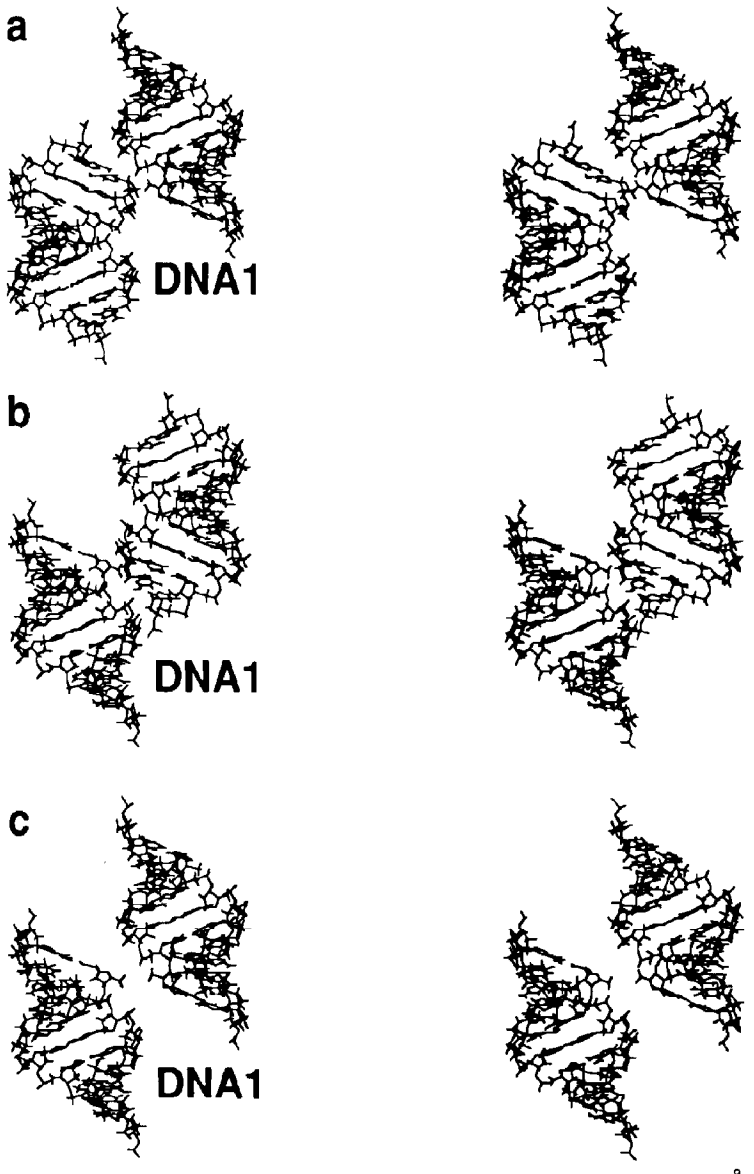

Fig. 11. Stereo views of the allowed intermolecular packing of A-DNA decamer Pairs where $\Delta x = -17$ Å, $\Delta y = 17$ Å, $\theta = 0°$, and (a) $\theta 1$, $\theta 2 = (-150°, 60°)$, (b) $\theta 1$, $\theta 2 = (120°, -120°)$, (c) $\theta 1$, $\theta 2 = (-150°, -120°)$, (d) $\theta 1$, $\theta 2 = (-90°, -120°)$, (e) $\theta 1$, $\theta 2 = (-150°, 180°)$. Packing arrangements correspond respectively to states *A-E* in Table 5.

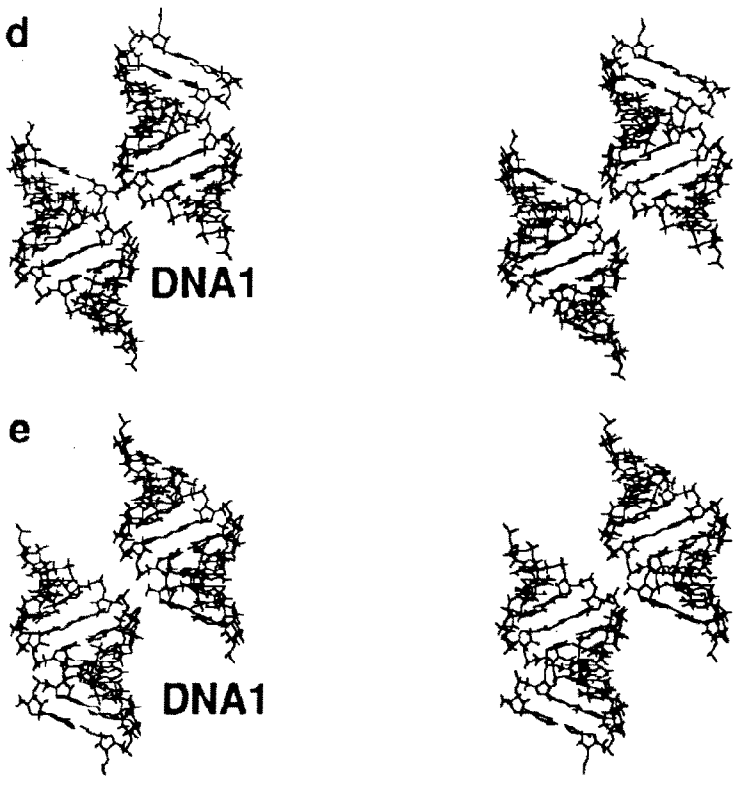

Fig. 11. (continued).

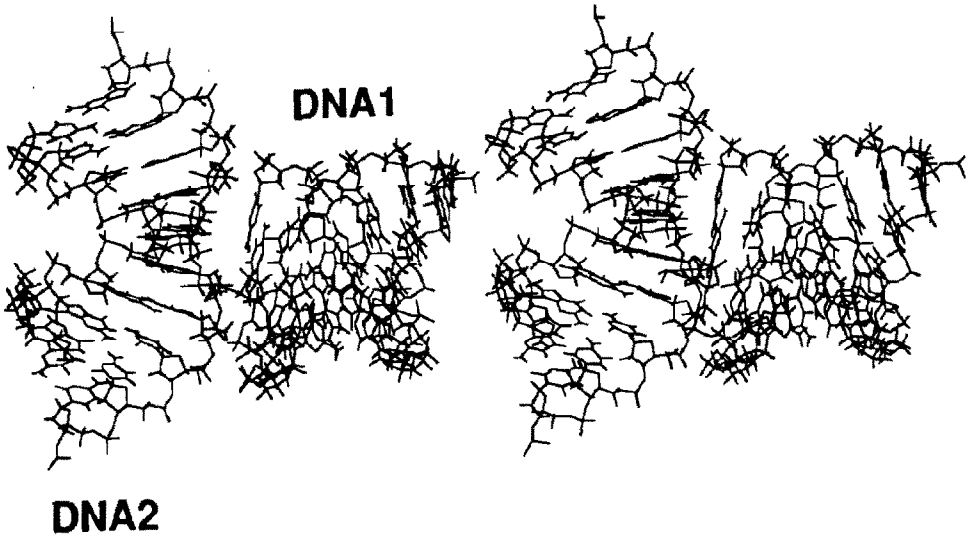

Fig. 12. Stereo representation of the allowed intermolecular packing of perpendicular ($\theta = 90°$) A-DNA decamer pairs with $\Delta x = 17$ Å, $\Delta y = 14$ Å, and $\theta 1, \theta 2 = (30°, 180°)$.

tions noted in Fig. 11(a) and 11(b), however, disappear when the A-DNA is increased in length.

The packing patterns predicted for the A-DNA decamer are quite different from the spatial arrangements of neighboring helices reported in several A-DNA crystals, where the terminal base pair of one helix stacks on the flat minor groove of its neighbor [37,39,62–64]. This packing motif is reproduced in the hard-sphere analysis if the A-DNA duplex pairs are oriented with helical axes describing roughly perpendicular angles. One such arrangement, corresponding to $\Delta x = 17$ Å, $\Delta y = 14$ Å, $\theta = 90°$, and $\theta 1$, $\theta 2 = (30°, 180°)$, is illustrated in Fig. 12. The terminal base pair of one of the A-DNA's is seen to stack on the flat minor groove of the other duplex. The tetragonal lattice predicted by repetition of this local packing motif in three successive $dG_{10} \cdot dC_{10}$ duplex pairs (i.e., A1 · A2, A2 · A3, A3 · A4), however, is sterically disallowed. Two of the A-DNA decamers (namely A1 and A4) are found to self-intersect in the higher order structure. This problem can be avoided if the A-DNA fragments are of shorter chain length or are displaced by larger values of Δx. It is interesting in this context to note that with the one exception of the d(CCCC-CGCGGGGG)$_2$ dodecamer [39], the A-DNA crystal structures solved to date are those of octamers rather than decamers. Duplexes of eight base pairs do not self-intersect when the local perpendicular pairwise packing motif is repeated in several neighbors. A large vertical displacement of neighboring A-DNA helices prevents the occurrence of unfavorable molecular contacts in the dodecamer crystal.

3.2.2 *Parallel packing of $dG_{20} \cdot dC_{20}$ A-DNA helices*

Packing calculations have also been performed with two 20-residue fragments of standard A-DNA ($dG_{20} \cdot dC_{20}$) in both parallel ($\theta = 0°$) and antiparallel ($\theta = 180°$) arrangements. The chains are fixed in various positions with the vertical slippage Δx adopting values of 0 ± 17 Å and the horizontal displacement Δy set at 20, 21, 22, 22.5, 23 Å. Contact maps corresponding to the parallel and antiparallel packing of the neighboring A-DNA helices with $\Delta x = 0$ Å and $\Delta y = 22.5$ Å are reported in Table 6. Two pathways of related contact-free or near contact-free states (i.e., less than six steric contacts) are apparent from the italicized boldface numbers in the table. It is noted that the directionality of the paths with respect to the $\theta 1$, $\theta 2$ variables is changed when the orientation of the interacting helices is reversed. When the chains are packed in a parallel fashion, there is a positive correlation between $\theta 1$ and $\theta 2$ over the allowed pathways, and when the chains are packed in an antiparallel fashion there is a negative correlation. The magnitudes of the differences in rotational variables $\theta 1 - \theta 2$, however, are comparable on the two maps. Assemblies of A-DNA's are expected to pack in hexagonal or square arrays based on the contact-free arrangements in Table 6 where $\theta 1 - \theta 2 = \pm 60°$ or $\pm 90°$, respectively. This prediction is consistent in principle, although not in detail, with the hexagonal and tetragonal lattices found in the A-DNA octamer crystals. As noted above, the helices are not aligned in parallel or antiparallel columns (i.e., $\theta = 0°$ or 180°) in the crystal structures. The helices, however, are aligned in parallel in the ideal A-DNA fiber model, although the duplexes are packed in a monoclinic unit cell with closest neighbors forming long molecular planes [46]. According to the hard-sphere calculations in Table 6, it is easier for the A-DNA 20-mers to pack in a parallel rather than an antiparallel arrangement when $\Delta x = 0$ Å and $\Delta y = 22.5$ Å. There are more contact-free (six versus two) and near contact-free (66 versus 59) arrangements of the parallel than the antiparallel pairs at this displacement.

Representative examples of the contact-free packing of parallel and antiparallel A-DNA 20-mers at the separation distances specified above are depicted in stereo in Fig. 13. The parallel ($\theta = 0°$) arrangement at the top of the figure is generated with the $\theta 1$, $\theta 2 = (180°, 90°)$ rotational combination and the antiparallel ($\theta = 180°$) arrangement at the bottom of the figure with the $\theta 1$, $\theta 2 = (-90°, 0°)$ state. Both representations in the figure are "back" views of the respective helix pairs. The two arrangements are seen to form extended "super" grooves comparable to those found above with shorter A-DNA fragments and

Table 6

$\theta 1$, $\theta 2$ Contact maps describing allowed spatial arrangements of parallel ($\theta = 0°$) and antiparallel ($\theta = 180°$) $dG_{20}\cdot dC_{20}$ A-DNA duplexes

$\Delta x = 0$ Å, $\Delta y = 22.5$ Å, $\theta = 0°$														
	0	23	25	9	*2*	*3*	25	22	24	8	*1*	*3*	9	23
	−30	24	7	*3*	*3*	19	24	25	*6*	*1*	*4*	9	25	24
	−60	*4*	*1*	*4*	13	24	19	*3*	*1*	*5*	*6*	22	25	*4*
	−90	*0*	*4*	14	24	13	*3*	*2*	*6*	11	25	25	*4*	*0*
	−120	*3*	12	25	14	*4*	*3*	9	16	20	25	*2*	*0*	*3*
↑	−150	9	25	12	*4*	*1*	7	25	20	19	*2*	*0*	*2*	9
$\theta 1(°)$	180	25	9	*3*	*0*	*4*	24	23	12	*5*	*3*	*4*	16	25
	150	16	*2*	*0*	*4*	25	25	9	*5*	*2*	8	11	25	16
	120	*4*	*0*	*2*	25	22	9	*3*	*2*	*5*	25	25	11	*4*
	90	*3*	*2*	25	25	*6*	*4*	*1*	*6*	25	25	25	8	*3*
	60	*5*	19	20	11	*5*	*1*	8	25	22	25	*5*	*2*	*5*
	30	12	20	16	*6*	*1*	*6*	24	18	25	*6*	*2*	*5*	12
	0	23	25	9	*2*	*3*	25	22	24	8	*1*	*3*	9	23
		0	30	60	90	120	150	180	−150	−120	−90	−60	−30	0
$\theta 2(°) \rightarrow$														
$\Delta x = 0$ Å, $\Delta y = 22.5$ Å, $\theta = 180°$														
	0	25	11	*6*	*2*	*3*	24	21	11	10	*2*	*4*	12	25
	−30	7	25	11	*5*	*2*	*2*	24	14	11	10	*2*	*2*	7
	−60	*3*	9	25	11	*6*	*2*	*3*	22	17	14	11	*1*	*3*
	−90	*0*	*3*	8	25	11	*5*	*2*	*2*	17	25	25	11	*0*
	−120	*4*	*2*	*2*	8	25	11	*6*	*4*	*2*	9	18	25	*4*
↑	−150	25	*6*	*2*	*3*	9	25	11	7	*2*	*2*	*5*	25	25
$\theta 1(°)$	180	25	25	*4*	*0*	*3*	7	25	25	8	*3*	*1*	*2*	25
	150	*2*	25	25	11	*1*	*2*	12	24	25	7	*1*	*2*	*2*
	120	*1*	*5*	18	25	11	*2*	*4*	8	19	25	8	*1*	*1*
	90	*3*	*2*	9	25	14	10	*2*	*4*	14	10	25	7	*3*
	60	8	*2*	*2*	17	17	11	10	*1*	8	14	19	25	8
	30	25	7	*4*	*2*	22	14	11	16	*1*	*4*	8	24	25
	0	25	11	*6*	*2*	*3*	24	21	11	10	*2*	*4*	12	25
		0	30	60	90	120	150	180	−150	−120	−90	−60	−30	0
$\theta 2(°) \rightarrow$														

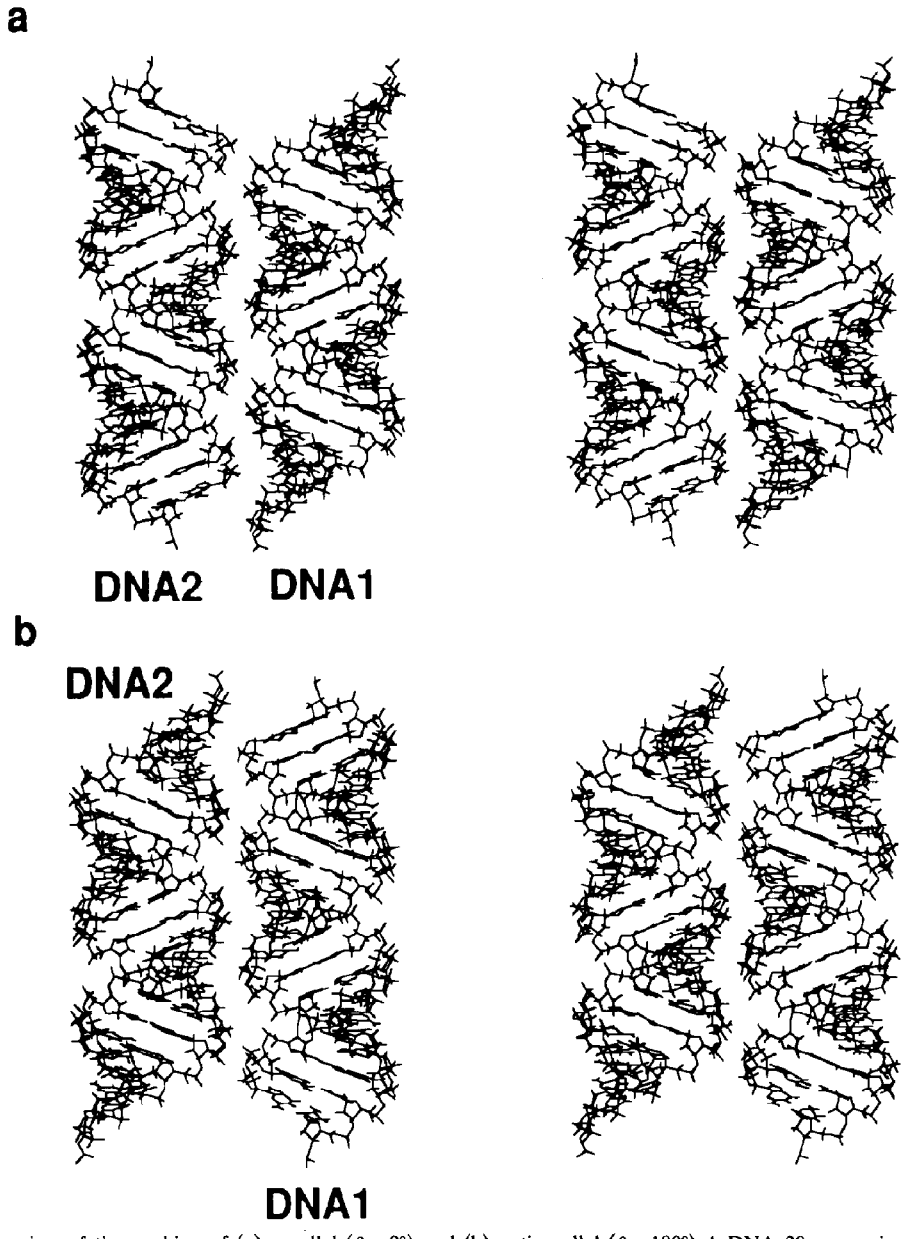

Fig. 13. Stereo view of the packing of (a) parallel ($\theta = 0°$) and (b) antiparallel ($\theta = 180°$) A-DNA 20-mer pairs, generated with horizontal displacement $\Delta y = 22.5$ Å, vertical slippage $\Delta x = 0$ Å, and intermolecular rotations $\theta 1$, $\theta 2 = (180°, 90°)$ and $(-90°, 0°)$, respectively.

with B-DNA. The empty space between the A-DNA pairs, however, is considerably smaller than the corresponding volume between closely packed B-DNA helices. This difference is apparently related to the displacement of base pairs with respect to the helical axes in A- versus B-DNA. An interesting cross pattern of stacked residues in the two A-DNA duplexes is also evident in Fig. 13. The pattern is a consequence of the inclination of A-DNA base pairs with respect to the

Table 7

$\theta 1$, $\theta 2$ Contact map describing allowed spatial arrangements of antiparallel d(CGCGCGCGCGCG)$_2$ Z-DNA duplexes

$\Delta x = 6.8$ Å, $\Delta y = 17$ Å, $\theta = 180°$													
	0	25	25	25	25	25	25	25	25	25	19	23	25	25
	−30	25	22	25	25	25	12	25	25	25	25	18	25	25
	−60	23	25	25	25	25	25	25	25	25	25	25	12	23
	−90	18	25	16	*6*	25	25	25	12	25	25	25	18	18
	−120	25	16	*2*	16	25	25	25	25	21	25	25	25	25
↑	−150	25	25	16	25	25	22	25	25	25	12	25	25	25
$\theta 1$(°)	180	25	25	25	18	23	25	25	25	25	21	25	25	25
	150	25	25	25	18	12	25	25	22	25	20	*0*	*2*	25
	120	25	25	25	25	25	18	23	25	25	16	8	*0*	25
	90	21	12	25	25	25	25	19	25	25	14	16	20	21
	60	25	25	21	25	25	25	25	19	23	25	25	25	25
	30	25	25	25	12	25	25	25	25	19	25	25	22	25
	0	25	25	25	25	25	25	25	25	25	19	23	25	25
		0	30	60	90	120	150	180	−150	−120	−90	−60	−30	0
$\theta 2$(°) →														
$\Delta x = -6.8$ Å, $\Delta y = 17$ Å, $\theta = 180°$														
	0	25	24	25	25	25	21	25	25	25	25	25	25	25
	−30	25	15	25	25	25	25	21	14	25	25	25	25	25
	−60	25	25	25	25	25	25	25	21	25	25	25	25	25
	−90	25	25	25	15	25	25	25	25	21	13	25	25	25
	−120	25	22	25	25	25	25	25	25	25	15	25	25	25
↑	−150	*1*	*6*	22	25	25	15	24	25	25	24	17	*4*	*1*
$\theta 1$(°)	180	*4*	*1*	25	25	25	25	25	17	25	25	25	15	*4*
	150	15	*4*	25	25	25	25	25	15	24	25	25	25	15
	120	25	17	25	25	25	25	25	25	25	25	25	25	25
	90	25	24	15	13	25	25	25	25	18	*2*	25	25	25
	60	25	25	25	21	25	25	25	22	17	18	25	24	25
	30	17	25	25	25	21	14	25	24	22	25	25	15	17
	0	25	24	25	25	25	21	25	25	25	25	25	25	25
		0	30	60	90	120	150	180	−150	−120	−90	−60	−30	0
$\theta 2$(°) →														

helical axes. Such a packing arrangement would be expected to give rise to a unique optical spectrum if present in a condensed DNA system [65].

3.3 Z-DNA

The antiparallel ($\theta = 180°$) packing of $d(CGCGCGCGCGCG)_2$ oligomers in the idealized Z-II helical conformation [42] is described by the contact maps in Table 7. The axes of the two double helices are laterally separated by a distance $\Delta y = 17$ Å and are vertically translated by displacements $\Delta x = \pm 16.8$ Å in these examples. Small clusters of near contact-free arrangements (with less than six disallowed contacts) of the Z-DNA helices are found in the two grids. These states are highlighted in boldface and italics in the table. The numbers of low contact configurations are somewhat different at positive and negative vertical displacements (five versus six at 6.8 Å and −6.8 Å, respectively), reflecting the dinucleotide repeat of the double helix. While there are no contact-free packing arrangements found when the chain ends are perfectly in register (i.e., $\Delta x = 0$ Å), there is one near contact-free state of the two Z-DNA's at this displacement when $\theta 1$, $\theta 2 = (-150°, 30°)$ (data not shown). The range of allowed configurations of neighboring Z-DNA's is quite different from the packing of B-DNA and A-DNA where there are no allowed packing arrangements at the same lateral and vertical separation distances. In the case of Z-DNA, the number of allowed packing configurations is roughly independent of the vertical slippage over the range $\Delta x = -17$ to 17 Å for a fixed interhelical orientation angle θ (see Table 4).

One of the packing motifs associated with the $\theta 1$, $\theta 2$ configurations of Z-DNA pairs noted above is illustrated in stereo in Fig. 14. The configuration in this example is the zero contact $\theta 1$, $\theta 2 = (150°, -60°)$ state from the $\Delta x = 6.8$ Å grid (top half of Table 7). This picture is a "front" view showing the convex major grooves of the two Z-DNA's in close contact and the concave minor

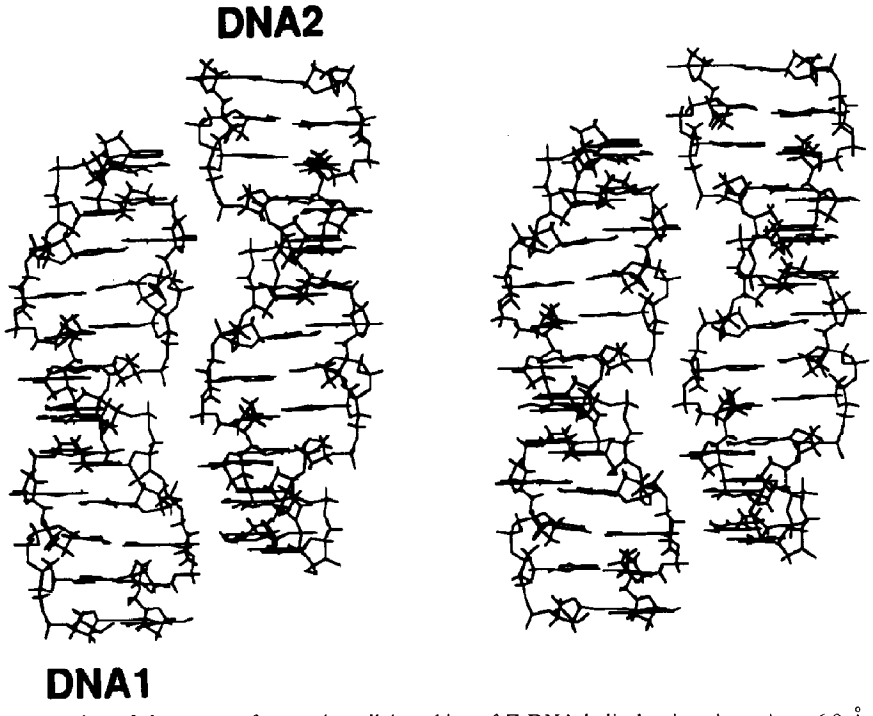

Fig. 14. Stereo representation of the contact-free antiparallel packing of Z-DNA helical pairs where $\Delta x = 6.8$ Å, $\Delta y = 17$ Å, $\theta 1$, $\theta 2 = (150°, -60°)$.

grooves positioned to form an extended "super" valley. The base-pairs projecting out of the convex groove of one of the Z-DNA's are in close contact with the sugar-phosphate backbone of the neighboring duplex. Side-by-side packing of this sort is also observed in the unit cell of the Z-DNA $d(CGCGCG)_2$ structure [66]. The displacement of neighboring duplexes along the helical axis, however, is somewhat greater in the crystal structure, the distance corresponding to roughly three base pairs or approximately 11 Å, versus 6.8 Å here. The closest approach of phosphorus atoms in neighboring duplexes is also somewhat smaller in the theoretical model than in the Z-DNA crystal structure (5.2 Å versus 6.9 Å). The DNA helices in the crystal are separated, on the other hand, by approximately the same distance (17 Å) as the duplexes in the hard-sphere model. The Z-DNA's in the crystal are associated laterally in a hexagonal close packing array. The pairwise packing motif in Fig. 14, however, cannot be extended to a molecular array. A third Z-DNA would be superimposed upon one of the original duplexes in the contact-free molecular pair.

Additional Z-DNA packing motifs are found with other sets of translational and rotational parameters in the hard-sphere calculations. For example, there are numerous sterically allowed side-by-side arrangements of Z-DNA dodecamers with inclined helical axes (see Table 4). As with B-DNA helices, these Z-DNA structures are able to pack more closely than either parallel or antiparallel helix pairs. In such structures, the convex groove of one Z-DNA is locked into the concave groove of the other duplex.

4. Summary

The Ramachandran hard-sphere contact criteria commonly used to assess intramolecular conformational flexibility account surprisingly well for various intermolecular packing motifs observed in X-ray structures of A-, B-, and Z-DNA. A number of configurations identified simply on the basis of hard-sphere interactions are in good agreement with the observed packing of DNA molecules in single crystal structures and fiber diffraction models. Successfully predicted associations include the antiparallel packing of neighboring duplexes in the B-DNA d(CGCGAATTCGCG) · (TGGCCGCGGTGT) dodecamer structure, the interlocked major groove base-phosphate backbone interactions in the d(ACCGGCGCCACA) · (TGGCCGCGGTGT) B-DNA crystal, the interdigitated arrangements of parallel B-DNA decamers in monoclinic and orthorhombic unit cells, the groove packing tendencies of short A-DNA fragments, and the side-by-side packing of Z-DNA helices. The pairwise interactions of neighboring helices appear to account as well for some of the higher-order three-dimensional packing patterns observed in X-ray studies. The sterically allowed screw rotations about neighboring B-DNA helical axes, for example, generate the square arrays of stacked columns found in the decamer crystal structures. The interhelical rotational alignments predicted by the hard-sphere analysis of A-DNA fragments are also in qualitative agreement with the tetragonal and hexagonal packing observed in A-DNA crystal structures.

Equally interesting in this study are the broad ranges of sterically acceptable arrangements of adjacent helices which do not satisfy the crystallographic symmetry requirements. Pathways of interdependent contact-free or near contact-free configurational changes (with six or fewer hard-sphere violations) are noted in the calculations. The rotational dispositions of neighboring duplexes are varied along some of these routes while the overall packing morphology is concomitantly preserved. These correlated arrangements are expected to be of comparable intermolecular energy and potentially interconvertible. Such pathways are consistent with the apparent twisting of DNA duplexes in liquid crystalline forms [21] as well as with the apparent disorder of some DNA's in the solid state [67]. Among the most interesting morphological features of the DNA packing predictions are the extended "super" grooves formed by the association of longer chain fragments. These grooves may facilitate the wrapping and packaging of DNA chains in supramolecular assemblies by serving as ligand binding sites or by acting as channels to concentrate mo-

bile counterions. As recently pointed out [59], the "super" grooves of neighboring DNA's may additionally act as nucleation sites for the higher order twisting of molecular layers in crystalline or concentrated liquid crystalline phases.

The hard-sphere packing computations also provide information relevant to the study of long-range intramolecular DNA–DNA interactions. The numerous allowed configurations of duplex pairs at crossed orientations, for example, are useful starting points for the all-atom modeling of DNA supercoils and cruciforms. According to the computed numbers of sterically acceptable configurations reported here, the association of A-, B-, and Z-DNA helical pairs is more likely at crossed orientations than in parallel or antiparallel arrangements. These local interactions might be relevant to the preferred configurations of long interwound DNA's or to the structures of four-stranded DNA junctions [56–58].

The hard-sphere packing analysis is, of course, limited by its very simplicity. The inferences that can be drawn from consideration of the steric interactions of DNA duplex pairs alone are insufficient for quantitative interpretation of the packing of double helices in the solid state. As noted above, the duplexes in crystal structures are often more widely spaced than the hard-sphere analysis predicts. The effects of bound solvent molecules and the specific interactions of hydrogen bonding must be explicitly considered to account for these discrepancies. The likelihood of a particular DNA–DNA packing motif is also not simply a function of the number of sterically allowed closely packed configurations of neighboring chains. Account must be taken of various contributions to the intermolecular energy, most notably the electrostatic interactions involving the negatively charged phosphate groups. Computations of this nature are in progress.

Acknowledgments

Sponsorship of this research by the U.S. Public Health Service under research grant GM-20861 is gratefully acknowledged. The authors are also grateful to Professor Helen M. Berman, Dr. Stephen L. Ginell, Dr. N. Narendra, and Dr. Bohdan Schneider for helpful discussions and for assistance in generating packing diagrams of DNA crystal structures, to Professor R. Chandrasekaran for information on DNA fiber packing, and to Professor Richard E. Dickerson and Professor Joel L. Sussman for sharing unpublished information on the packing of crystalline B-DNA decamers. Calculations were performed at the Rutgers Center for Computational Chemistry. Stereo figures were generated using the CHEM-X molecular modeling package [68].

References

1 F. Livolant, Eur. J. Cell Biol. 33 (1984) 300.
2 F. Livolant, J. Phys. (Les Ulis) 48 (1987) 1051.
3 F. Livolant and M.F. Maestre, Biochemistry 27 (1988) 3056.
4 N.Z. Namaradze, A.N. Goryunov and T.M. Birshtein, Biophys. Chem. 7 (1977) 59.
5 J.L. Sussman and E.N. Trifonov, Proc. Natl. Acad. Sci. USA 75 (1978) 103.
6 M. Levitt, Proc. Natl. Acad. Sci. USA 75 (1978) 640.
7 T.J. Richmond, J.T. Finch, B. Rushton, D. Rhodes and A. Klug, Nature 311 (1984) 532.
8 M. Ptashne, Nature 322 (1986) 697.
9 A.R. Srinivasan, R. Torres, W. Clark and W.K. Olson, J. Biomol. Struct. Dynam. 5 (1987) 459.
10 L.E. Ulanovsky and E.N. Trifonov, Nature 326 (1987) 720.
11 R.C. Maroun and W.K. Olson, Biopolymers 27 (1988) 585.
12 H.-S. Koo and D.M. Crothers, Proc. Natl. Acad. Sci. USA 85 (1988) 1763.
13 A. Bolshoy, P. McNamara, R.E. Harrington and E.N. Trifonov, Proc. Natl. Acad. Sci. USA 88 (1991) 2312.
14 M.J.B. Tunis-Schneider and M.F. Maestre, J. Mol. Biol. 52 (1970) 521.
15 L.S. Lerman, Proc. Natl. Acad. Sci. USA 68 (1971) 1886.
16 C.F. Jordan, L.S. Lerman and J.H. Venable, Nature New Biol. 236 (1972) 67.
17 F. Livolant, J. Phys. (Les Ulis) 47 (1986) 1605.
18 T.E. Strzelecka, M.W. Davidson and R.L. Rill, Nature 331 (1988) 457.
19 R.L. Rill, F. Livolant, H.C. Aldrich and M.W. Davidson, Chromosoma 98 (1989) 280.
20 F. Livolant, A.M. Levelut, J. Doucet and J.P. Benoit, Nature 339 (1989) 724.
21 R. Brandes and D.R. Kearns, J. Phys. Chem. 92 (1988) 6836.
22 D.H. Van Winkle, M.W. Davidson, W.-X. Chen and R.L. Rill, Macromolecules 23 (1990) 4140.
23 D.C. Rau, B. Lee and V.A. Parsegian, Proc. Natl. Acad. Sci. USA 81 (1984) 2621.

24 S. Trohalaki, H.L. Frisch and L.S. Lerman, Biophys. Chem. 40 (1991) 197.
25 K.A. Marx and G.C. Ruben, J. Biomol. Struct. Dynam. 4 (1986) 23.
26 T.E. Strzelecka and R.L. Rill, Macromolecules 24 (1991) 514.
27 W.C. Earnshaw, J. King, S.C. Harrison and F.A. Eiserling, Cell 14 (1978) 559.
28 R.E. Dickerson, D.S. Goodsell, M.L. Kopka and P.E. Pjura, J. Biomol. Struct. Dynam. 5 (1987) 557.
29 R.E. Dickerson, K. Grzeskowiak, M. Grzeskowiak, M.L. Kopka, T. Larsen, A. Lipanov, G.G. Privé, J. Quintana, P. Schultze, K. Yanagi, H. Yuan and H.-C. Yoon, Nucleosides Nucleotides 10 (1991) 3.
30 U. Heinemann and C. Alings, J. Mol. Biol. 210 (1989) 369.
31 G.G. Privé, K. Yanagi and R.E. Dickerson, J. Mol. Biol. 217 (1991) 177.
32 K. Grzeskowiak, K. Yanagi, G.G. Privé and R.E. Dickerson, J. Biol. Chem. 266 (1991) 8861.
33 Y. Timsit, E. Westhof, R.P.P. Fuchs and D. Moras, Nature 341 (1989) 459.
34 M. Miller, R.W. Harrison, A. Wlodawer, E. Appella and J.L. Sussman, Nature 334 (1988) 85.
35 L. Joshua-Tor, D. Rabinovich, H. Hope, F. Frolow, E. Appella and J.L. Sussman, Nature 334 (1988) 82.
36 L. Joshua-Tor, F. Frolow, E. Appella, H. Hope, D. Rabinovich and J.L. Sussman, J. Mol. Biol., in press.
37 Z. Shakked and O. Kennard, in: Structure of biological macromolecules and assemblies, Vol 2: Nucleic acids and interactive proteins, eds. F. Jurnak and A. McPherson (Wiley, New York, NY, 1985) p. 1.
38 U. Heinemann, J. Biomol. Struct. Dynam. 8 (1991) 801.
39 N. Verdaguer, J. Aymamí, D. Fernández-Forner, I. Fita, M. Coll, T. Huynh-Dinh, J. Igolen and J.A. Subirana, J. Mol. Biol. 221 (1991) 623.
40 W. Saenger, Principles of nucleic acids structure (Springer-Verlag, New York, NY, 1984).
41 A.H.-J. Wang and M.-K. Teng, J. Cryst. Growth 90 (1988) 295.
42 A.H.-J. Wang, G.J. Quigley, F.J. Kolpak, G. van der Marel, J.H. van Boom and A. Rich, Science 211 (1981) 171.
43 R. Langridge, H.R. Wilson, C.W. Hooper, M.H.F. Wilkins and L.D. Hamilton, J. Mol. Biol. 2 (1960) 19.
44 S. Arnott and D.W.L. Hukins, Biochim. Biophys. Res. Commun. 47 (1972) 1504.
45 R. Chandrasekaran and S. Arnott in: Landolt-Börnstein numerical data and functional relationships in science and technology, Group VII/1b, Nucleic acids, ed. W. Saenger (Springer-Verlag, Berlin, 1989) p. 31.
46 R. Chandrasekaran, M. Wang, R.-G. He, L.C. Puigjaner, M.A. Byler, R.P. Millane and S. Arnott, J. Biomol. Struct. Dynam. 6 (1989) 1189.
47 A.D. Buckingham, P.W. Fowler and J.M. Hutson, Chem. Rev. 88 (1988) 963.
48 J.M. Hutson, Annu. Rev. Phys. Chem. 41 (1990) 123.
49 G.N. Ramachandran, C.R. Ramakrishnan and V. Sasisekharan, J. Mol. Biol. 7 (1963) 95.
50 V. Sasisekharan, A.V. Lakshminarayanan and G.N. Ramachandran in: Conformation of Biopolymers 2, ed. G.N. Ramachandran (Academic Press, New York, NY, 1967) p. 641.
51 W.K. Olson and P.J. Flory, Biopolymers 11 (1972) 1.
52 A.L. Mazanov and M.A. Mokul'skii, Mol. Biol. USSR (Eng. ed.) 9 (1975) 389.
53 G.J. Thomas Jr. and P. Serwer, J. Raman Spectrosc. 21 (1990) 569.
54 Z. Reich, R. Ghirlando and A. Minsky, Biochemistry 30 (1991) 7828.
55 M.-H. Hao and W.K. Olson, J. Biomol. Struct. Dynam. 7 (1990) 661.
56 M.E.A. Churchill, T.D. Tullius, N.R. Kallenbach and N.C. Seeman, Proc. Natl. Acad. Sci. USA 85 (1988) 4653.
57 J.P. Cooper and P.J. Hagerman, Proc. Natl. Acad. Sci. USA 86 (1989) 7336.
58 A.I.H. Murchie, R.M. Clegg, E. von Kitzing, D.R. Duckett, S. Diekmann and D.M.J. Lilley, Nature 341 (1989) 763.
59 F. Livolant, J. Mol. Biol. 218 (1991) 165.
60 H.R. Drew, R.M. Wing, T. Takano, C. Broka, S. Tanaka, K. Itakura and R.E. Dickerson, Proc. Natl. Acad. Sci. USA 78 (1981) 2179.
61 H.R. Drew and R.E. Dickerson, J. Mol. Biol. 151 (1981) 535.
62 Z. Shakked, D. Rabinovich, W.B.T. Cruse, E. Egert, O. Kennard, G. Sala, S.A. Salisbury and M.A. Viswamitra, Proc. R. Soc. B213 (1981) 479.
63 A.H.-J. Wang, S. Fujii, J.H. van Boom and A. Rich, Proc. Natl. Acad. Sci. USA 79 (1982) 3968.
64 S. Jain, G. Zon and M. Sundaralingam, Biochemistry 30 (1991) 3567.
65 I. Tobias, Biopolymers 23 (1984) 1315.
66 A.H.-J. Wang, G.J. Quigley, F.J. Kolpak, J.L. Crawford, J.H. van Boom, G. van der Marel and A. Rich, Nature 282 (1979) 680.
67 J. Doucet, J.-P. Benoit, W.B.T. Cruse, T. Prange and O. Kennard, Nature 337 (1989) 190.
68 E.K. Davies, CHEM-X program suite (Chemical Design, Ltd., Oxford, 1986).